World Electric Vehicle Journal

MDPI

Article

A Novel Robust H_∞ Control Approach Based on Vehicle Lateral Dynamics for Practical Path Tracking Applications

Jie Wang [1], Baichao Wang [1], Congzhi Liu [2,*], Litong Zhang [1] and Liang Li [3]

[1] School of Mechanical and Electrical Engineering, Changchun University of Science and Technology, Changchun 130022, China; 2021100498@mails.cust.edu.cn (J.W.); 2016800048@cust.edu.cn (B.W.); zhanglitong@cust.edu.cn (L.Z.)
[2] School of Mechanical and Vehicle Engineering, Chongqing University, Chongqing 400044, China
[3] State Key Laboratory of Automotive Safety and Energy, Tsinghua University, Beijing 100084, China; liangl@tsinghua.edu.cn
* Correspondence: liucongzhi@cqu.edu.cn

Abstract: This paper proposes a robust lateral control scheme for the path tracking of autonomous vehicles. Considering the discrepancies between the model parameters and the actual values of the vehicle and the fluctuation of parameters during driving, the norm-bounded uncertainty is utilized to deal with the uncertainty of model parameters. Because some state variables in the model are difficult to measure, an H_∞ observer is designed to estimate state variables and provide accurate state information to improve the robustness of path tracking. An H_∞ state feedback controller is proposed to suppress system nonlinearity and uncertainty and produce the desired steering wheel angle to solve the path tracking problem. A feedforward control is designed to deal with road curvature and further reduce tracking errors. In summary, a path tracking method with H_∞ performance is established based on the linear matrix inequality (LMI) technique, and the gains in observer and controller can be obtained directly. The hardware-in-the-loop (HIL) test is built to validate the real-time processing performance of the proposed method to ensure excellent practical application potential, and the effectiveness of the proposed control method is validated through the utilization of urban road and highway scenes. The experimental results indicate that the suggested control approach can track the desired trajectory more precisely compared with the model predictive control (MPC) method and make tracking errors within a small range in both urban and highway scenarios.

Keywords: autonomous path tracking; lateral dynamic control; H_∞ control; parameter uncertainty; LMI

Citation: Wang, J.; Wang, B.; Liu, C.; Zhang, L.; Li, L. A Novel Robust H_∞ Control Approach Based on Vehicle Lateral Dynamics for Practical Path Tracking Applications. *World Electr. Veh. J.* **2024**, *15*, 293. https://doi.org/10.3390/wevj15070293

Academic Editor: Joeri Van Mierlo

Received: 5 February 2024
Revised: 21 June 2024
Accepted: 25 June 2024
Published: 30 June 2024

1. Introduction

Autonomous driving is becoming increasingly feasible with the development of critical technologies like steering-by-wire, artificial intelligence, and others [1,2]. The development of autonomous driving technology can effectively reduce traffic accidents caused by various human factors, improve the efficiency of traffic operation, and alleviate the problem of traffic congestion, while taking the driver out of mechanized driving and making the driving process comfortable [3,4].

Longitudinal and lateral dynamics controls are essential components of autonomous driving and are typically considered separately or in a coupled way [5]. Lateral dynamics control, which uses automatic steering to keep the vehicle near the desired trajectory within a sensitive error range, has been the subject of several research studies, and many control schemes have been established, such as proportion integration differentiation (PID) control [6], fuzzy control [7], sliding mode control [8], linear quadratic regulator (LQR) control [9], model predictive control (MPC) [10], and H_∞ control [11]. Multiple fuzzy inference engines were used to design the steering controller, and the stability condition was given in [7]. A sliding mode-based state observer was proposed to estimate the side

slip angle, and an adaptive sliding mode controller was designed to calculate the corrected steering angle in [8]. A dangerous potential field was constructed to generate a desired trajectory for collision avoidance, and the multi-constrained MPC controller is designed to achieve path tracking in [10]. Since the vehicle lateral control is a comparatively complex problem, which needs more robustness to ensure safety [12], and since it is well-known that the H_∞ control method has an excellent ability to deal with structural perturbation and outside interference [13], it has been applied to improve path tracking performance.

A robust output-feedback controller was designed, and particular uncertainties and disturbances of the autonomous race car caused by limit driving or chassis adjustments are considered in the controller design in [14]. The observer-based finite frequency H_∞ controller was proposed in [15], and the linear parameter varying (LPV) model was utilized to formulate the nonlinear path tracking system, in which the vehicle speed variable is taken into account. The experimental results demonstrate that this control method is superior to the full-frequency control in terms of tracking performance. Ref. [16] presented a robust H_∞ output-feedback control strategy, which employed the mixed genetic algorithm to obtain control gain that satisfies linear matrix inequality (LMI) and realizes path following. A lateral control system with fuzzy state observer based on the Takagi–Sugeno fuzzy model of four-wheel independent vehicles was proposed, and H_∞ state feedback control was adopted to produce the desired front wheel steering angle and external yaw moment in [17]. A LPV/H_∞ controller was designed to generate the front and rear wheel steering angles and external yaw moment for autonomous ground vehicles, and the weighted least square (WLS) allocation algorithm was utilized to achieve torque allocation between the left and right side wheels in [18]. An H_∞ output feedback control method considering input delay and tire saturation was proposed in [19]. To increase the robustness of the controller, the uncertainty of tire cornering stiffness and external disturbance were considered. A robust H_∞ fault-tolerant controller was proposed in [20]. The dynamic model also takes actuator loss-of-effectiveness and bias fault into account in addition to parameter uncertainty. In addition to the design of the H_∞ controller, the author treats the input data dropouts as random binary numbers that form a Bernoulli distribution to deal with the issue of unreliable communication links in [21]. The backlash-type hysteresis of the steering system was considered, and the H_∞ controller was designed in [22]. The above H_∞ control methods partially address the issues of parameter uncertainty and outside interference, while the LPV model was utilized to deal with the challenge of system nonlinearity. Further, some studies consider the issues of signal delay and loss of the steering system.

Nevertheless, the majority of the above literature only took into account the uncertainty of two or three model parameters and the others are ignored, which is not desirable. The primary objective of this paper is to devise a robust observer and controller in a decoupled manner, while considering the uncertainties associated with all parameters. The method of decoupling is employed to mitigate the complexity of the solution, as it proves challenging to address the problem when there is a coupling between the observer and controller. Meanwhile, the quantity, weight, and placement of passengers have a significant impact on the vehicle's mass, the location of the mass center, and the moment of inertia, which is particularly significant in severe circumstances and can seriously affect the performance of path tracking. Hence, it is necessary to consider the uncertainty of all parameters to improve the robustness and performance of path tracking.

Compared with the previous research, the main contributions of this paper are summarized as follows:

1. The uncertainty of vehicle mass, tire cornering stiffness, the length from the center of gravity (CG) to the front and rear wheel axles, longitudinal velocity, and moment of inertia are considered, and the norm-bounded uncertainty is utilized to deal with them in the design of a dynamic model. Then, a quasi-linear system with uncertainty is established for the vehicle dynamics control.

2. In order to restrain the nonlinearity and uncertainty of the system, the design criteria of the H_∞ observer and controller are established and can be utilized for path tracking and other lateral control fields.
3. A feedforward control approach is designed, which includes adaptive feedforward to deal with road curvature and proportional feedforward to further reduce tracking errors. Then, a robust lateral control performance can be obtained for its practical application.

The overall lateral control process is shown in Figure 1, and the structure of this paper is organized as follows. Section 2 describes the lateral dynamics model and explains the treatment of parameter uncertainty. In Sections 3 and 4, the derivation process of the H_∞ observer and controller is described in detail. In Section 5, the feedforward control is proposed to suppress static errors. In Section 6, the simulation based on Prescan-Simulink and an analysis of the results is presented. Finally, a brief conclusion to this paper is provided in Section 7.

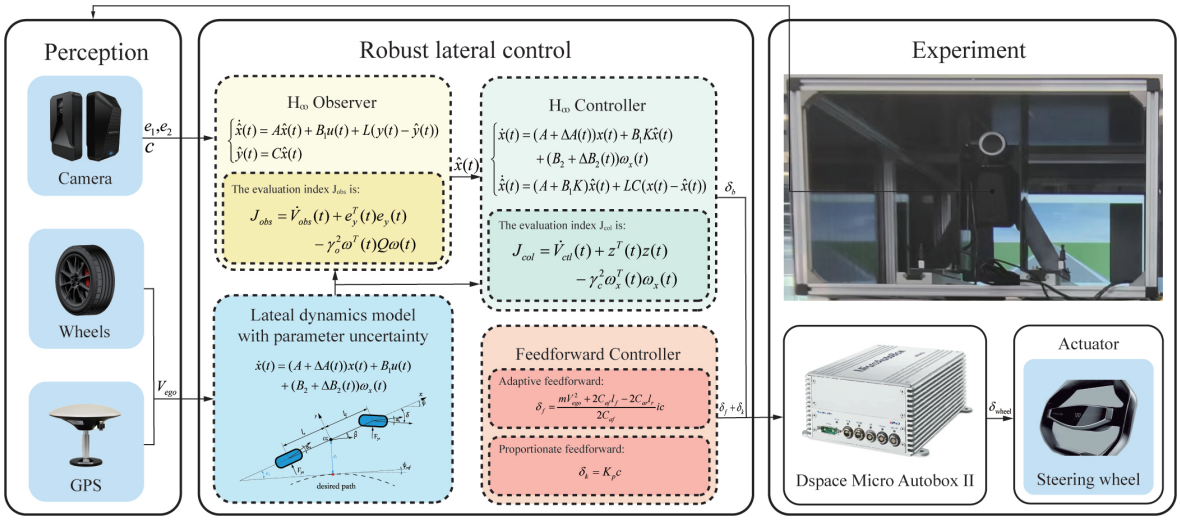

Figure 1. Structure diagram of the robust lateral control system.

2. System Design

2.1. Lateral Dynamics Model

Vehicle models can be divided into kinematic models based on geometric relations [23] and dynamic models based on mechanical relationships, taking tire characteristics into consideration. Kinematic models are typically applied at low velocities. The tire's sideways characteristics are disregarded because of their weak force. While the vehicle is moving at a faster speed, the lateral force on the vehicle cannot be neglected. The dynamics models provide a more accurate description of the vehicle's turning characteristics.

The lateral dynamics model of 4-wheel-steering vehicles is established based on the 2-DoF dynamics model [24], and it is more efficient for path tracking because it is constructed in the Frenet coordinate system, which incorporates road information. When the rear wheel angle of the vehicle is 0, neglecting the second derivative of desired vehicle yaw rate $\ddot{\psi}_{ref}$ and incorporating $\dot{\psi}_{ref} = V_{ego}c$, as shown in Figure 2, the lateral dynamics model of front-wheel steering vehicles can be expressed as follows, and the definitions of symbols are listed in Table 1:

$$\dot{\tilde{X}} = \tilde{A}\tilde{X} + \tilde{B}_1\delta + \tilde{B}_2 c, \tag{1}$$

where

$$\tilde{X} = \begin{bmatrix} e_1 & \dot{e_1} & e_2 & \dot{e_2} \end{bmatrix}^T,$$

$$\tilde{A} = \begin{bmatrix} 0 & 1 & 0 & 0 \\ 0 & -\frac{2C_{af}+2C_{ar}}{mV_{ego}} & \frac{2C_{af}+2C_{ar}}{m} & -\frac{2C_{af}l_f-2C_{ar}l_r}{mV_{ego}} \\ 0 & 0 & 0 & 1 \\ 0 & -\frac{2C_{af}l_f-2C_{ar}l_r}{I_zV_{ego}} & \frac{2C_{af}l_f-2C_{ar}l_{ar}}{I_z} & -\frac{2C_{af}l_f^2+2C_{ar}l_r^2}{I_zV_{ego}} \end{bmatrix},$$

$$\tilde{B_1} = \begin{bmatrix} 0 \\ \frac{2C_{af}}{m} \\ 0 \\ \frac{2C_{af}l_f}{I_z} \end{bmatrix}, \tilde{B_2} = \begin{bmatrix} 0 \\ -V_{ego}^2 - \frac{2C_{af}l_f-2C_{ar}l_r}{m} \\ 0 \\ -\frac{2C_{af}l_f^2+2C_{ar}l_r^2}{I_z} \end{bmatrix}.$$

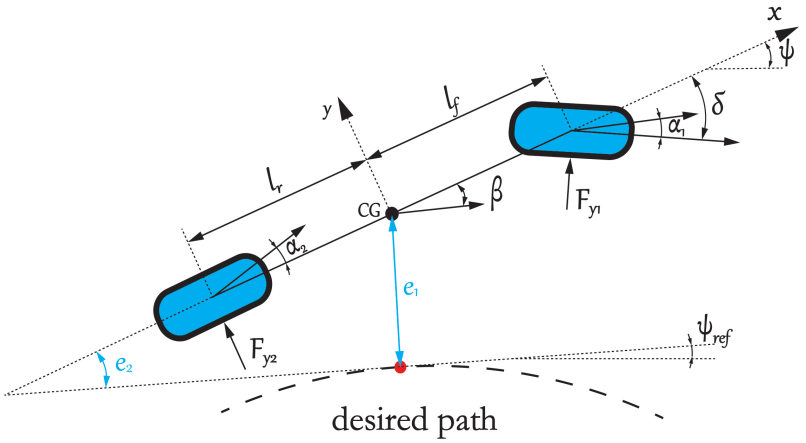

Figure 2. Lateral dynamics model.

Table 1. Symbols and descriptions for the dynamics model.

Description	Symbol	Unit
Vehicle mass	m	kg
Vehicle yaw moment of inertia	I_z	m/s^2
Cornering stiffness of front/rear tires	C_{af}, C_{ar}	N/rad
Distance from CG to front/rear axle	l_f, l_r	m
Vehicle longitudinal speed	V_{ego}	m/s
Center of vehicle gravity	CG	
Vehicle side slip angle	β	rad
Front wheel angle	δ	rad
Speed deflection angle of front/rear wheel	α_1, α_2	rad
Lateral force on front/rear wheel	F_{y1}, F_{y2}	N
Yaw angle of vehicle	ψ	rad
Desired orientation of vehicle	ψ_{ref}	rad
Lateral distance error from the CG to the reference trajectory	e_1	m
Heading angle error	e_2	rad
Path curvature	c	m^{-1}

Since the steering system has a significant impact on the performance of path tracking, the first-order inertia element is appended to take into account the actual steering system's delay property, with the front wheel angle serving as the state variable, and the steering wheel angle representing the input. Then, Equation (1) can be rewritten as:

$$\frac{d}{d_t}\begin{bmatrix}\tilde{X}\\ \delta\end{bmatrix}=\begin{bmatrix}\tilde{A} & \tilde{B_1}\\ 0 & -\frac{1}{\tau}\end{bmatrix}\begin{bmatrix}\tilde{X}\\ \delta\end{bmatrix}+\begin{bmatrix}0\\ \frac{1}{\tau i}\end{bmatrix}u+\begin{bmatrix}\tilde{B_2}\\ 0\end{bmatrix}c, \tag{2}$$

where τ is the time constant of the first order process, i represents the steering system's transmission ratio, and c denotes the curvature of the ideal path. Since τ and i can be obtained through online calibration by the steering-by-wire system of the vehicle, their uncertainties can be disregarded.

Remark 1. *The lateral dynamic model is a linear time-invariant (LTI) model, which assumes that the longitudinal speed is constant. In this paper, it can be considered that the system is quasi-linear in the future control domain, and the dynamics model is switched according to the velocity interval to replace the LPV model. Then, the computational efficiency is improved, and the real-time performance of the algorithm is guaranteed.*

2.2. Description of System Uncertainty

The path curvature c can be regarded as an external disturbance ω_x in the design of the observer and controller, since it is typically small in cases of high speed. The visual sensor can directly measure the lateral distance error e_1 and heading error e_2. Meanwhile, considering the uncertainty of vehicle parameters, the system in Equation (2) can be described as:

$$\begin{cases}\dot{x}(t)=(A+\Delta A(t))x(t)+B_1u(t)\\ \qquad\quad +(B_2+\Delta B_2(t))\omega_x(t)\\ y(t)=Cx(t),\end{cases} \tag{3}$$

where

$$x=\begin{bmatrix}\tilde{X}\\ \delta\end{bmatrix},A=\begin{bmatrix}\tilde{A} & \tilde{B_1}\\ 0 & -\frac{1}{\tau}\end{bmatrix},B_1=\begin{bmatrix}0\\ \frac{1}{\tau i}\end{bmatrix},$$
$$B_2=\begin{bmatrix}\tilde{B_2}\\ 0\end{bmatrix},C=\begin{bmatrix}1 & 0 & 0 & 0 & 0\\ 0 & 0 & 1 & 0 & 0\end{bmatrix}.$$

The perturbed matrices $\Delta A(\cdot), \Delta B_2(\cdot)$ are expressed in the following form:

$$\begin{cases}\Delta A(t)=H_1N(t)E_1\\ \Delta B_2(t)=H_2N(t)E_2\end{cases}, \tag{4}$$

where $N(t)$ is an unknown matrix function representing uncertainty which satisfies $N^T(t)N(t)\leq I$, and I is the identity matrix of the appropriate dimension. The inequality $N^T(t)N(t)\leq I$ implies that the uncertainty of the parameters in the model must not surpass the fluctuation range of the respective parameters.

Next, the construction process of H_1, E_1, H_2, and E_2 in Equation (4) will be discussed in detail.

Since the parameters of mass, velocity, and moment of inertia are present in the denominator, higher-order uncertainty will be generated. To avoid this, all parameters are represented via the norm-bounded uncertainty [25]:

$$\begin{aligned}&C_{\text{af}}=C_{fe}+N(t)\bar{C}_{fn},\\ &C_{\text{ar}}=C_{re}+N(t)\bar{C}_{rn},\\ &l_f=l_{fe}+N(t)\bar{l}_{fn},\\ &l_r=l_{re}+N(t)\bar{l}_{rn},\\ &V_{ego}=V_{moe}+N(t)\bar{V}_{mon},\end{aligned} \tag{5}$$

where

$$
\begin{aligned}
C_{fe} &= \frac{C_{f\max} + C_{f\min}}{2}, \bar{C}_{fn} = \frac{C_{f\max} - C_{f\min}}{2},\\
C_{re} &= \frac{C_{r\max} + C_{r\min}}{2}, \bar{C}_{rn} = \frac{C_{r\max} - C_{r\min}}{2},\\
l_{fe} &= \frac{l_{f\max} + l_{f\min}}{2}, \bar{l}_{fn} = \frac{l_{f\max} - l_{f\min}}{2},\\
l_{re} &= L - l_{fe}, \bar{l}_{rn} = -\bar{l}_{fn},\\
V_{moe} &= \frac{V_{\max} + V_{\min}}{2}, V_{mon} = \frac{V_{\max} - V_{\min}}{2},
\end{aligned}
$$

where $C_{f\max}$ and $C_{r\max}$ represent the maximum tire cornering stiffness of the front and rear wheels; $C_{f\min}$ and $C_{r\min}$ represent the minimum tire cornering stiffness of the front and rear wheels, which can be obtained by fitting experimental data; $l_{f\max}$ and $l_{f\min}$ denote the maximum and minimum distance between the front axle and the center of gravity; $V_{\max}$ and $V_{\min}$ are the maximum and minimum estimate of the vehicle's current speed, respectively; and L represents the wheelbase between the front and rear axles of the vehicle.

Similarly, using the maximum and minimum estimates of the current vehicle speed $V_{\max}$, $V_{\min}$, maximum mass $m_{\max}$, minimum mass $m_{\min}$, maximum rotational inertia $I_{z\max}$, and minimum rotational inertia $I_{z\min}$, the uncertain vehicle speed, mass, and rotational inertia can be expressed as:

$$
\begin{aligned}
\tfrac{1}{V_{ego}} &= V_e + N(t)\bar{V}_n,\\
\tfrac{1}{m} &= m_e + N(t)\bar{m}_n,\\
\tfrac{1}{I_z} &= I_e + N(t)\bar{I}_n,
\end{aligned}
\tag{6}
$$

where

$$
\begin{aligned}
V_e &= \frac{1}{2}(V_{s\max} + V_{s\min}), \bar{V}_n = \frac{1}{2}(V_{s\max} - V_{s\min}),\\
V_{s\max} &= \frac{1}{V_{\min}}, V_{s\min} = \frac{1}{V_{\max}},\\
m_e &= \frac{1}{2}(m_{s\max} + m_{s\min}), \bar{m}_n = \frac{1}{2}(m_{s\max} - m_{s\min}),\\
m_{s\max} &= \frac{1}{m_{\min}}, m_{s\min} = \frac{1}{m_{\max}},\\
I_e &= \frac{1}{2}(I_{zs\max} + I_{zs\min}), \bar{I}_n = \frac{1}{2}(I_{zs\max} - I_{zs\min}),\\
I_{zs\max} &= \frac{1}{I_{z\min}}, I_{zs\min} = \frac{1}{I_{z\max}}.
\end{aligned}
$$

It is noteworthy that the values at both ends of Equation (6) are approximately equivalent. As the difference between $V_{\max}$ and $V_{\min}$ decreases, the value on the right side of Equation (6) is closer to the value on the left.

For the representation of the system in Equation (3), uncertain terms $\frac{C_{af}+C_{ar}}{mV_{ego}}$ can be written as Equation (7), and others are described in Appendix A.

$$
\begin{aligned}
\frac{C_{af}+C_{ar}}{mV_{ego}} &= \Big[\Big(C_{fe} + N(t)\bar{C}_{fn}\Big) + (C_{re} + N(t)\bar{C}_{rn})\Big](m_e + N(t)\bar{m}_n)(V_e + N(t)\bar{V}_n)\\
&= \Big[\Big(C_{fe} + C_{re}\Big) + \Big(\bar{C}_{fn} + \bar{C}_{rn}\Big)N(t)\Big]\Big[m_eV_e + (m_e\bar{V}_n + V_e\bar{m}_n)N(t) + \bar{m}_n\bar{V}_nN^2(t)\Big]\\
&= \Big(C_{fe} + C_{re}\Big)m_eV_e + \Big[\Big(C_{fe} + C_{re}\Big)(m_e\bar{V}_n + V_e\bar{m}_n) + \Big(\bar{C}_{fn} + \bar{C}_{rn}\Big)m_eV_e\Big]N(t)\\
&\quad + \Big[\Big(C_{fe} + C_{re}\Big)\bar{m}_n\bar{V}_n + \Big(\bar{C}_{fn} + \bar{C}_{rn}\Big)(m_e\bar{V}_n + V_e\bar{m}_n)\Big]N^2(t) + \Big(\bar{C}_{fn} + \bar{C}_{rn}\Big)\bar{m}_n\bar{V}_nN^3(t)
\end{aligned}
\tag{7}
$$

Note that $|N(t)| \leq 1$, where $|\cdot|$ represents the absolute value. Thus, the higher-order term of $N(t)$ is relatively smaller or equal to its first-order term, and then Equation (7) is approximated as:

$$\frac{C_{af} + C_{ar}}{mV_{ego}} \approx \left(C_{fe} + C_{re}\right) m_e V_e + \Delta_1 N(t), \tag{8}$$

where

$$\begin{aligned}\Delta_1 = &\left(C_{fe} + C_{re}\right)(m_e \bar{V}_n + V_e \bar{m}_n + \bar{m}_n \bar{V}_n) \\ &+ \left(\bar{C}_{fn} + \bar{C}_{rn}\right)(m_e V_e + m_e \bar{V}_n + V_e \bar{m}_n + \bar{m}_n \bar{V}_n),\end{aligned}$$

and H_1, E_1, H_2, and E_2 can be defined as:

$$H_1 = \begin{bmatrix} 0 & 0 & 0 & 0 & 0 \\ 0 & -2\Delta_1 & 2\Delta_2 & -2\Delta_3 & 2\Delta_4 \\ 0 & 0 & 0 & 0 & 0 \\ 0 & -2\Delta_5 & 2\Delta_6 & -2\Delta_7 & 2\Delta_8 \\ 0 & 0 & 0 & 0 & 0 \end{bmatrix}, E_1 = I_{5\times 5},$$

$$H_2 = \begin{bmatrix} 0 & 0 & 0 & 0 & 0 \\ -\Delta_9 & 0 & 0 & 0 & 0 \\ 0 & 0 & 0 & 0 & 0 \\ -2\Delta_{10} & 0 & 0 & 0 & 0 \\ 0 & 0 & 0 & 0 & 0 \end{bmatrix}, E_2 = \begin{bmatrix} 1 \\ 1 \\ 1 \\ 1 \\ 1 \end{bmatrix},$$

where

$$\begin{aligned}
\Delta_2 &= \left(C_{fe} + C_{re}\right)\bar{m}_n + \left(\bar{C}_{fn} + \bar{C}_{rn}\right)(m_e + \bar{m}_n), \\
\Delta_3 &= \zeta_1 m_e V_e + \left(C_{fe} l_{fe} - C_{re} l_{re} + \zeta_1\right)(m_e \bar{V}_n + V_e \bar{m}_n + \bar{m}_n \bar{V}_n), \\
\Delta_4 &= C_{fe} \bar{m}_n + m_e \bar{C}_{fn} + \bar{C}_{fn} \bar{m}_n, \\
\Delta_5 &= \zeta_1 I_e V_e + \left(C_{fe} l_{fe} - C_{re} l_{re} + \zeta_1\right)(I_e \bar{V}_n + V_e \bar{I}_n + \bar{I}_n \bar{V}_n), \\
\Delta_6 &= \zeta_1 I_e + \left(C_{fe} l_{fe} - C_{re} l_{re} + \zeta_1\right)\bar{I}_n, \\
\Delta_7 &= \zeta_2 I_e V_e + \left(C_{fe} l_{fe}^2 + C_{re} l_{re}^2 + \bar{C}_{fn} \bar{l}_{fn}^2 + \bar{C}_{rn} \bar{l}_{rn}^2 + \zeta_2\right) \\
&\quad (I_e \bar{V}_n + V_e \bar{I}_n) + \left(\bar{C}_{fn} \bar{l}_{fn}^2 + \bar{C}_{rn} \bar{l}_{rn}^2 + \zeta_2\right)\bar{I}_n \bar{V}_n, \\
\Delta_8 &= \left(C_{fe} \bar{l}_{fn} + l_{fe} \bar{C}_{fn} + \bar{C}_{fn} \bar{l}_{fn}\right) I_e + \left(C_{fe} l_{fe} + C_{fe} \bar{l}_{fn} + l_{fe} \bar{C}_{fn} + \bar{C}_{fn} \bar{l}_{fn}\right)\bar{I}_n, \\
\Delta_9 &= 2\zeta_1 m_e + 2\left(C_{fe} l_{fe} - C_{re} l_{re} + \zeta_1\right)\bar{m}_n + 2V_{moe} \bar{V}_{mon} + \bar{V}_{mon}^2, \\
\Delta_{10} &= \left(l_{fe}^2 \bar{l}_{fn} + l_{re}^2 \bar{l}_{rn} + \zeta_3\right) I_e + \left(C_{fe} l_{fe}^2 + C_{re} l_{re}^2 + l_{fe}^2 \bar{C}_{fn} + l_{re}^2 \bar{C}_{rn} + \zeta_3\right)\bar{I}_n, \\
\zeta_1 &= C_{fe} \bar{l}_{fn} + l_{fe} \bar{C}_{fn} - C_{re} \bar{l}_{rn} - l_{re} \bar{C}_{rn} + \bar{C}_{fn} \bar{l}_{fn} - \bar{C}_{rn} \bar{l}_{rn}, \\
\zeta_2 &= 2C_{fe} l_{fe} \bar{l}_{fn} + 2C_{re} l_{re} \bar{l}_{rn} + \bar{C}_{fn} l_{fe}^2 + \bar{C}_{rn} l_{re}^2 \\
&\quad + C_{fe} \bar{l}_{fn}^2 + C_{re} \bar{l}_{rn}^2 + 2\bar{C}_{fn} \bar{l}_{fn} l_{fe} + 2\bar{C}_{rn} \bar{l}_{rn} l_{re}, \\
\zeta_3 &= 2C_{fe} l_{fe} \bar{l}_{fn} + 2C_{re} l_{re} \bar{l}_{rn} + C_{fe} \bar{l}_{fn} + C_{re} \bar{l}_{rn} \\
&\quad + 2l_{fe} \bar{l}_{fn} \bar{C}_{fn} + 2l_{re} \bar{l}_{rn} \bar{C}_{rn} + \bar{C}_{fn} \bar{l}_{fn} + \bar{C}_{rn} \bar{l}_{rn}.
\end{aligned}$$

Remark 2. *In order to improve the robustness of the system, the uncertainty of all parameters in the model is taken into consideration and processed by norm-bounded uncertainty. Furthermore, a quasi-linear system is established for the design of the H_∞ criteria.*

3. Design of the H-Infinity Observer

The accuracy of model parameter estimation has a direct impact on vehicle control effectiveness, but obtaining accurate parameters for the vehicle dynamics model is challenging in reality. Traditional optimal control optimizes control inputs based on known model parameter assumptions, but actual parameter estimation errors can be significant. Achieving better tracking performance requires a complex process of parameter adjustment, which can be effectively addressed by robust control methods.

It is assumed that the road curvature can be accurately detected, which indicates that the path curvature is regarded as a known variable [26]. Since some state variables are difficult to measure and the physical systems are uncertain and perturbed [27], the following H_∞ observer is established to provide accurate state estimates to improve the performance and robustness of path tracking and ensure that all state variables can be effectively used for feedback to produce the desired control input:

$$\begin{cases} \dot{\hat{x}}(t) = A\hat{x}(t) + B_1 u(t) + L(y(t) - \hat{y}(t)) \\ \hat{y}(t) = C\hat{x}(t) \end{cases}, \tag{9}$$

where L is the observer gain, and $\hat{x}(t)$ and $\hat{y}(t)$ are the estimates of $x(t)$ and $y(t)$.

When the observer error is designed to be $e_x(t) = x(t) - \hat{x}(t)$, the error system can be depicted as follows:

$$\begin{cases} \dot{e}_x(t) = (A - LC)e_x(t) + \Gamma\omega(t) \\ e_y(t) = Ce_x(t) \end{cases}, \tag{10}$$

where $\Gamma = \begin{bmatrix} \Delta A & B_2 + \Delta B_2 \end{bmatrix}$ and $\omega(t) = \begin{bmatrix} x^T(t) & \omega_x^T(t) \end{bmatrix}^T$. Since the H_∞ observer and H_∞ controller are coupled, it is necessary to solve bilinear matrix inequalities (BMIs) to obtain feedback gain, which is a challenging task. Therefore, the H_∞ observer and H_∞ controller are designed and solved separately in this paper. Here, $x(t)$ can be assumed to be bounded, which will be proved in the next section.

In order to obtain the H_∞ design criteria, the necessary lemma is given as follows:

Lemma 1 ([28]). *For any real matrices H and E, the following property holds for any positive scalar* $\epsilon > 0$*:*

$$HN(t)E + E^T N^T(t) H^T \leq \varepsilon HH^T + \frac{1}{\varepsilon} E^T E. \tag{11}$$

Then, an observer design criterion is proposed as shown below to suppress disturbance and ensure accurate estimation of the state observer.

Theorem 1. *If scale* $\gamma_o > 0$ *exists and the following inequality is satisfied:*

$$\begin{bmatrix} \Theta & 0 & P_o B_2 & C^T & P_o H_1 & P_o H_2 & 0 & 0 \\ * & -\bar{\gamma}_o \rho_1 & 0 & 0 & 0 & 0 & \epsilon_1 E_1^T & 0 \\ * & * & -\bar{\gamma}_o \rho_2 & 0 & 0 & 0 & 0 & \epsilon_2 E_2^T \\ * & * & * & -I & 0 & 0 & 0 & 0 \\ * & * & * & * & -\epsilon_1 I & 0 & 0 & 0 \\ * & * & * & * & * & -\epsilon_2 I & 0 & 0 \\ * & * & * & * & * & * & -\epsilon_1 I & 0 \\ * & * & * & * & * & * & * & -\epsilon_2 I \end{bmatrix} < 0 \tag{12}$$

where $\Theta = A^T P_o - C^T \xi^T + P_o A - \xi C$, $\bar{\gamma}_o = \gamma_o^2$,
then it has the solution: $P_o = P_o^T > 0$, $\bar{\gamma}_o > 0$, $\epsilon_1 > 0$, $\epsilon_2 > 0$, $\xi = P_o L$. *Then, the* H_∞ *performance is true:*

$$\int_0^T \| e_y(t) \|^2 dt < \lambda_{\max}(P_o) \| e_x(0) \|^2 + \gamma_o^2 \int_0^T \omega^T(t) Q \omega(t) dt, \tag{13}$$

where $\lambda_{\max}(P_o)$ is the largest eigenvalue of a positive definite matrix P_o, $Q = diag(\rho_1, \rho_2)$, and ρ_1 and ρ_2 are the weight coefficients of $x(t)$ and $\omega_x^T(t)$, respectively.

Proof of Theorem 1. The Lyapunov function is proposed as $V_{obs} = e_x^T(t)P_o e_x(t)$; then:

$$\begin{aligned}
\dot{V}_{obs}(t) =& \dot{e}_x^T(t)P_o e_x(t) + e_x^T(t)P_o \dot{e}_x(t) \\
=& [e_x^T(t)(A-LC)^T + \omega^T(t)\Gamma^T]P_o e_x(t) \\
&+ e_x^T(t)P_o[(A-LC)e_x(t) + \Gamma\omega(t)] \\
=& \begin{bmatrix} e_x(t) \\ \omega(t) \end{bmatrix}^T \begin{bmatrix} \kappa & P_o\Gamma \\ \Gamma^T P_o & 0 \end{bmatrix} \begin{bmatrix} e_x(t) \\ \omega(t) \end{bmatrix} \\
=& \begin{bmatrix} e_x(t) \\ x(t) \\ \omega_x(t) \end{bmatrix}^T \begin{bmatrix} \kappa & 0 & P_o B_2 \\ 0 & 0 & 0 \\ B_2^T P_o & 0 & 0 \end{bmatrix} \begin{bmatrix} e_x(t) \\ x(t) \\ \omega_x(t) \end{bmatrix} \\
&+ \begin{bmatrix} e_x(t) \\ x(t) \\ \omega_x(t) \end{bmatrix}^T \begin{bmatrix} 0 & P_o\Delta A & P_o\Delta B_2 \\ \Delta A^T P_o & 0 & 0 \\ \Delta B_2^T P_o & 0 & 0 \end{bmatrix} \begin{bmatrix} e_x(t) \\ x(t) \\ \omega_x(t) \end{bmatrix},
\end{aligned} \tag{14}$$

where $\kappa = (A-LC)^T P_o + P_o(A-LC)$.

The term in the second half of $\dot{V}_{obs}$ is used to represent the uncertain parameter part of the system. From Lemma 1 given above in Equation (11), it can be rewritten as:

$$\begin{aligned}
&\begin{bmatrix} 0 & P_o\Delta A & P_o\Delta B_2 \\ \Delta A^T P_o & 0 & 0 \\ \Delta B_2^T P_o & 0 & 0 \end{bmatrix} \\
\le& \varepsilon_1^{-1} \begin{bmatrix} P_o H_1 \\ 0 \\ 0 \end{bmatrix} \begin{bmatrix} P_o H_1 \\ 0 \\ 0 \end{bmatrix}^T + \varepsilon_1 \begin{bmatrix} 0 \\ E_1^T \\ 0 \end{bmatrix} \begin{bmatrix} 0 \\ E_1^T \\ 0 \end{bmatrix}^T \\
&+ \varepsilon_2^{-1} \begin{bmatrix} P_o H_2 \\ 0 \\ 0 \end{bmatrix} \begin{bmatrix} P_o H_2 \\ 0 \\ 0 \end{bmatrix}^T + \varepsilon_2 \begin{bmatrix} 0 \\ 0 \\ E_2^T \end{bmatrix} \begin{bmatrix} 0 \\ 0 \\ E_2^T \end{bmatrix}^T.
\end{aligned} \tag{15}$$

In order to establish the H_∞ performance (13), the evaluation index J_{obs} is given as follows:

$$\begin{aligned}
J_{obs} =& \dot{V}_{obs}(t) + e_y^T(t)e_y(t) - \gamma_o^2 \omega^T(t) Q \omega(t) \\
\le& \begin{bmatrix} e_x(t) \\ x(t) \\ \omega_x(t) \end{bmatrix}^T \begin{bmatrix} \theta & 0 & P_o B_2 \\ 0 & -\gamma_o^2\rho_1 & 0 \\ B_2^T P_o & 0 & -\gamma_o^2\rho_2 \end{bmatrix} \begin{bmatrix} e_x(t) \\ x(t) \\ \omega_x(t) \end{bmatrix} \\
&+ \begin{bmatrix} e_x(t) \\ x(t) \\ \omega_x(t) \end{bmatrix}^T \begin{bmatrix} C^T \\ 0 \\ 0 \end{bmatrix} \begin{bmatrix} C^T \\ 0 \\ 0 \end{bmatrix}^T \begin{bmatrix} e_x(t) \\ x(t) \\ \omega_x(t) \end{bmatrix} + \begin{bmatrix} e_x(t) \\ x(t) \\ \omega_x(t) \end{bmatrix}^T \\
&\left\{ \varepsilon_1 \begin{bmatrix} 0 \\ E_1^T \\ 0 \end{bmatrix} \begin{bmatrix} 0 \\ E_1^T \\ 0 \end{bmatrix}^T + \varepsilon_2 \begin{bmatrix} 0 \\ 0 \\ E_2^T \end{bmatrix} \begin{bmatrix} 0 \\ 0 \\ E_2^T \end{bmatrix}^T \right\} \begin{bmatrix} e_x(t) \\ x(t) \\ \omega_x(t) \end{bmatrix} \\
=& \begin{bmatrix} e_x(t) \\ x(t) \\ \omega_x(t) \end{bmatrix}^T \Pi \begin{bmatrix} e_x(t) \\ x(t) \\ \omega_x(t) \end{bmatrix},
\end{aligned} \tag{16}$$

where $\theta = A^T P_o - C^T L^T P_o + P_o A - P_o LC + \epsilon_1^{-1} P_o H_1 H_1^T P_o + \epsilon_2^{-1} P_o H_2 H_2^T P_o$.

Note that $\Pi < 0$ is equivalent to $J_{obs} < 0$. By the Schur complement [29], $\Pi < 0$ can be transformed into the LMI in Equation (12). It follows that:

$$\int_0^T \left[\dot{V}_{obs}(t) + e_y^T(t)e_y(t) - \gamma_o^2\omega^T(t)Q\omega(t)\right]dt < 0, \tag{17}$$

where

$$\int_0^T \dot{V}_{obs}(t)dt = V_{obs}(T) - V_{obs}(0) > -\lambda_{max}(P_o)\|e_x(0)\|^2.$$

Then, we can obtain the H_∞ performance (13), and the proof is completed. □

4. Design of the H-Infinity Controller

In the actual control process, the sensor-obtained information is subject to interference and fluctuations, and there is a delay in transmitting the control input from the controller to the actuator. These challenges can be effectively addressed through feedback control. However, feedforward control fails to overcome external interferences, requires precise model information, and has limited efficacy in enhancing tracking performance. Therefore, research primarily focuses on the design of the feedback controller.

In order to ensure the robustness of vehicle lateral dynamics control, suppress the nonlinearity and uncertainty of the dynamics model, and improve the performance of path tracking, an H_∞ control scheme based on the above observer is proposed. Defining $u(t) = K\hat{x}(t)$ and according to Equations (3) and (9), the state space model of the closed-loop system is described as:

$$\begin{cases} \dot{x}(t) = (A + \Delta A(t))x(t) + B_1K\hat{x}(t) \\ \qquad\quad + (B_2 + \Delta B_2(t))\omega_x(t) \\ \dot{\hat{x}}(t) = (A + B_1K)\hat{x}(t) + LC(x(t) - \hat{x}(t)). \end{cases} \tag{18}$$

Considering the observer error $e_x(t) = x(t) - \hat{x}(t)$, the augmented vector is defined as $\bar{X}(t) = \begin{bmatrix} x^T(t) & e_x^T(t) \end{bmatrix}^T$, and the augmented closed-loop system can be written as:

$$\begin{cases} \dot{\bar{X}}(t) = \bar{A}\bar{X}(t) + \bar{B}\omega_x(t) \\ \bar{Y}(t) = \bar{C}\bar{X}(t), \end{cases} \tag{19}$$

where the system matrix is as follows:

$$\bar{A} = \begin{bmatrix} A + \Delta A + B_1K & -B_1K \\ \Delta A & A - LC \end{bmatrix},$$
$$\bar{B} = \begin{bmatrix} B_2 + \Delta B_2 \\ B_2 + \Delta B_2 \end{bmatrix}, \bar{C} = \begin{bmatrix} I & 0 \end{bmatrix}.$$

Next, a controller design criterion is given as follows.

Theorem 2. *If $\gamma_c > 0$ exists and the following inequality is satisfied:*

$$\begin{bmatrix} \Omega_1 & -B_1K & B_2 & B_1K & vP_{inv1} & P_{inv1} & v_1H_1 & v_2H_2 & P_{inv1}E_1^T & 0 \\ * & \Omega_2 & P_2B_2 & 0 & 0 & 0 & v_1P_2H_1 & v_2P_2H_2 & 0 & 0 \\ * & * & -\bar{\gamma}_cI & 0 & 0 & 0 & 0 & 0 & 0 & E_2^T \\ * & * & * & -vI & 0 & 0 & 0 & 0 & 0 & 0 \\ * & * & * & * & -vI & 0 & 0 & 0 & 0 & 0 \\ * & * & * & * & * & -I & 0 & 0 & 0 & 0 \\ * & * & * & * & * & * & -v_1I & 0 & 0 & 0 \\ * & * & * & * & * & * & * & -v_2I & 0 & 0 \\ * & * & * & * & * & * & * & * & -v_1I & 0 \\ * & * & * & * & * & * & * & * & * & -v_2I \end{bmatrix} < 0, \tag{20}$$

it has the solution $P_{inv1} = P_{inv1}^T > 0$, $P_2 = P_2^T > 0$, $\bar{\gamma}_c > 0$, $\bar{\alpha} > 0$, $v > 0$, $v_1 > 0$, $v_2 > 0$, *where* $\Omega_1 = P_{inv1}A^T + AP_{inv1} - \bar{\alpha}I$, $\Omega_2 = A^T P_2 - C^T L^T P_2 + P_2 A - P_2 LC$, $\bar{\alpha} = \alpha^2$, $\bar{\gamma}_c = \gamma_c^2$. *Then, the* H_∞ *performance is true:*

$$\begin{aligned} \int_0^T \| \bar{Y}(t)\|^2 dt &< \lambda_{\max}(P_{c1}) \| x(0)\|^2 \\ &+ \lambda_{\max}(P_{c2}) \| e_x(0)\|^2 + \gamma_c^2 \int_0^T \| \omega_x(t)\|^2 dt \end{aligned} \tag{21}$$

where $\lambda_{\max}(P_c)$ *is the largest eigenvalue of a positive definite matrix* P_c .

Proof of Theorem 2. The Lyapunov function is designed to be $V_{ctl} = \bar{X}^T(t)P_c\bar{X}(t)$, and then its derivative is shown as follows:

$$\begin{aligned} \dot{V}_{ctl}(t) &= \dot{\bar{X}}^T(t)P_c\bar{X}(t) + \bar{X}^T(t)P_c\dot{\bar{X}}(t) \\ &= \bar{X}^T(t)(\bar{A}^T P_c + P_c\bar{A})\bar{X}(t) + \omega_x^T(t)\bar{B}^T P_c\bar{X}(t) \\ &+ \bar{X}^T(t)P_c\bar{B}\omega_x(t), \end{aligned} \tag{22}$$

where the matrix P_c is defined as $P_{c1} \oplus P_{c2}$.

Then, the specific expression of $\dot{V}_{ctl}(t)$ is as follows:

$$\begin{aligned} \dot{V}_{ctl}(t) = &\begin{bmatrix} x(t) \\ e_x(t) \\ \omega_x(t) \end{bmatrix}^T \begin{bmatrix} \theta_1 & \theta_2 & P_{c1}B_2 \\ \theta_2^T & \theta_3 & P_{c2}B_2 \\ B_2^T P_{c1} & B_2^T P_{c2} & 0 \end{bmatrix} \begin{bmatrix} x(t) \\ e_x(t) \\ \omega_x(t) \end{bmatrix} \\ &+ \begin{bmatrix} x(t) \\ e_x(t) \\ \omega_x(t) \end{bmatrix}^T \begin{bmatrix} \theta_4 & \theta_5 & \theta_6 \\ \theta_5^T & 0 & \theta_7 \\ \theta_6^T & \theta_7^T & 0 \end{bmatrix} \begin{bmatrix} x(t) \\ e_x(t) \\ \omega_x(t) \end{bmatrix}, \end{aligned} \tag{23}$$

where $\theta_1 = A^T P_{c1} + K^T B_1^T P_{c1} + P_{c1}A + P_{c1}B_1 K$, $\theta_2 = -P_{c1}B_1 K$, $\theta_3 = A^T P_{c2} - C^T L^T P_{c2} + P_{c2}A - P_{c2}LC$, $\theta_4 = \Delta A^T(t)P_{c1} + P_{c1}\Delta A^T(t)$, $\theta_5 = \Delta A^T(t)P_{c2}$, $\theta_6 = P_{c1}\Delta B_2(t)$, $\theta_7 = P_{c2}\Delta B_2(t)$.

The uncertain parameter part of the system can be rewritten as:

$$\begin{aligned} &\begin{bmatrix} \Delta A^T(t)P_{c1} + P_{c1}\Delta A^T(t) & \Delta A^T(t)P_{c2} & P_{c1}\Delta B_2(t) \\ P_{c2}\Delta A(t) & 0 & P_{c2}\Delta B_2(t) \\ \Delta B_2^T(t)P_{c1} & \Delta B_2^T(t)P_{c2} & 0 \end{bmatrix} \\ &\le v_1 \begin{bmatrix} P_{c1}H_1 \\ P_{c2}H_1 \\ 0 \end{bmatrix} \begin{bmatrix} P_{c1}H_1 \\ P_{c2}H_1 \\ 0 \end{bmatrix}^T + v_1^{-1} \begin{bmatrix} E_1^T \\ 0 \\ 0 \end{bmatrix} \begin{bmatrix} E_1^T \\ 0 \\ 0 \end{bmatrix}^T \\ &+ v_2 \begin{bmatrix} P_{c1}H_2 \\ P_{c2}H_2 \\ 0 \end{bmatrix} \begin{bmatrix} P_{c1}H_2 \\ P_{c2}H_2 \\ 0 \end{bmatrix}^T + v_2^{-1} \begin{bmatrix} 0 \\ 0 \\ E_2^T \end{bmatrix} \begin{bmatrix} 0 \\ 0 \\ E_2^T \end{bmatrix}^T. \end{aligned} \tag{24}$$

The evaluation index J_{col1} is indicated as the following:

$$J_{col1} = \dot{V}_{ctl}(t) + \bar{Y}^T(t)\bar{Y}(t) - \gamma_c^2\omega_x^T(t)\omega_x(t). \tag{25}$$

According to Equations (19) and (22), it can be deduced that Equation (25) satisfies the following inequality:

$$
\begin{aligned}
J_{col1} \leq & \begin{bmatrix} x(t) \\ e_x(t) \\ \omega_x(t) \end{bmatrix}^T \begin{bmatrix} \eta_1 & \eta_2 & P_{c1}B_2 \\ \eta_2^T & \eta_3 & P_{c2}B_2 \\ B_2^T P_{c1} & B_2^T P_{c2} & -\gamma_c^2 I \end{bmatrix} \\
& \begin{bmatrix} x(t) \\ e_x(t) \\ \omega_x(t) \end{bmatrix} + \begin{bmatrix} x(t) \\ e_x(t) \\ \omega_x(t) \end{bmatrix}^T \begin{bmatrix} I \\ 0 \\ 0 \end{bmatrix} \begin{bmatrix} I \\ 0 \\ 0 \end{bmatrix}^T \begin{bmatrix} x(t) \\ e_x(t) \\ \omega_x(t) \end{bmatrix} \\
& + \begin{bmatrix} x(t) \\ e_x(t) \\ \omega_x(t) \end{bmatrix}^T \left\{ v_1^{-1} \begin{bmatrix} E_1^T \\ 0 \\ 0 \end{bmatrix} \begin{bmatrix} E_1^T \\ 0 \\ 0 \end{bmatrix}^T \right. \\
& \left. + v_2^{-1} \begin{bmatrix} 0 \\ 0 \\ E_2^T \end{bmatrix} \begin{bmatrix} 0 \\ 0 \\ E_2^T \end{bmatrix}^T \right\} \begin{bmatrix} x(t) \\ e_x(t) \\ \omega_x(t) \end{bmatrix} \\
= & \begin{bmatrix} x(t) \\ e_x(t) \\ \omega_x(t) \end{bmatrix}^T \psi \begin{bmatrix} x(t) \\ e_x(t) \\ \omega_x(t) \end{bmatrix},
\end{aligned} \tag{26}
$$

where $\eta_1 = A^T P_{c1} + K^T B_1^T P_{c1} + P_{c1} A + P_{c1} B_1 K + v_1 P_{c1} H_1 H_1^T P_{c1} + v_2 P_{c1} H_2 H_2^T P_{c1}$, $\eta_2 = -P_{c1} B_1 K + v_1 P_{c1} H_1 H_1^T P_{c2} + v_2 P_{c1} H_2 H_2^T P_{c2}$, $\eta_3 = A^T P_{c2} - C^T L^T P_{c2} + P_{c2} A - P_{c2} L C + v_1 P_{c2} H_1 H_1^T P_{c2} + v_2 P_{c2} H_2 H_2^T P_{c2}$.

Since the inequality $\psi < 0$ is nonlinear, it needs to be transformed into an LMI. Multiply the matrix $P_{c1}^{-1} \oplus I \oplus I$ to the left and right of the ψ, and P_{inv1} is defined as the inverse of matrix P_{c1}: $P_{c1}^{-1} \oplus I \oplus I = P_{inv1} \oplus I \oplus I$.

According to Lemma 1 in Equation (11) and noting that $\| v P_{inv1} - B_1 K \| \neq 0$, the existence of $\alpha > 0$ makes the following inequality true:

$$
v P_{inv1} P_{inv1} + v^{-1} B_1 K K^T B_1^T - \alpha^2 I \geq B_1 K P_{inv1} + P_{inv1} K^T B_1^T, \tag{27}
$$

where $\alpha > 0$ is utilized to ensure that inequality $\psi < 0$ is true and to avoid $\psi \leq 0$.

Then, $J_{col1} < 0$ is equivalent to $J_{col2} < 0$, where

$$
\begin{aligned}
J_{col2} = & \begin{bmatrix} \Xi_1 & \Xi_2 & B_2 \\ \Xi_2^T & \Xi_3 & P_{c2}B_2 \\ B_2^T & B_2^T P_{c2} & -\gamma_c^2 I \end{bmatrix} + \begin{bmatrix} P_{inv1} \\ 0 \\ 0 \end{bmatrix} \begin{bmatrix} P_{inv1} \\ 0 \\ 0 \end{bmatrix}^T \\
& + v_1^{-1} \begin{bmatrix} P_{inv1} E_1^T \\ 0 \\ 0 \end{bmatrix} \begin{bmatrix} P_{inv1} E_1^T \\ 0 \\ 0 \end{bmatrix}^T + v_2^{-1} \begin{bmatrix} 0 \\ 0 \\ E_2^T \end{bmatrix} \begin{bmatrix} 0 \\ 0 \\ E_2^T \end{bmatrix}^T
\end{aligned} \tag{28}
$$

and $\Xi_1 = P_{inv1} A^T + A P_{inv1} + v P_{inv1} P_{inv1} + v^{-1} B_1 K K^T B_1^T - \alpha^2 I + v_1 H_1 H_1^T + v_2 H_2 H_2^T$, $\Xi_2 = -P_{c1} B_1 K + v_1 H_1 H_1^T P_{c2} + v_2 H_2 H_2^T P_{c2}$, $\Xi_3 = A^T P_{c2} - C^T L^T P_{c2} + P_{c2} A - P_{c2} L C + v_1 P_{c2} H_1 H_1^T P_{c2} + v_2 P_{c2} H_2 H_2^T P_{c2}$.

According to the Schur complement, the equivalent condition $J_{col2} < 0$ can be transformed to the LMI as in Equation (20). It follows that:

$$
\int_0^T \left[\dot{V}_{ctl}(t) + \bar{Y}^T(t) \bar{Y}(t) - \gamma_c^2 \omega_x^T(t) \omega_x(t) \right] dt < 0 \tag{29}
$$

where

$$
\begin{aligned}
\int_0^T \dot{V}_{ctl}(t) dt &= V_{ctl}(T) - V_{ctl}(0) \\
&> -\lambda_{max}(P_{c1}) \| x(0) \|^2 - \lambda_{max}(P_{c2}) \| e_x(0) \|^2.
\end{aligned}
$$

Then, we can obtain the H_∞ performance (21), and the proof is completed. □

Remark 3. *It can be seen from Equation (19) that $\bar{Y}(t)$ in the above inequality (21) and the state variable $x(t)$ are equivalent. The inequality above indicates that $\bar{Y}(t)$ is bounded, which is consistent with the assumption when designing the observer that the state variable $x(t)$ is bounded. Then, the inequality (13) of the observer can be further written as:*

$$\begin{aligned}\int_0^T \| e_y(t)\|^2 dt < \lambda_{\max}(P_o) \| e_x(0)\|^2 \\ + \gamma_o^2 \rho_1 \int_0^T \| x(t)\|^2 dt + \gamma_o^2 \rho_2 \int_0^T \| \omega_x(t)\|^2 dt.\end{aligned} \tag{30}$$

According to Equations (21) and (30), we have

$$\begin{aligned}\int_0^T \| e_y(t)\|^2 dt < \gamma_o^2 \rho_1 \lambda_{max}(P_{c1}) \| x(0)\|^2 \\ + \left[\lambda_{\max}(P_o) + \gamma_o^2 \rho_1 \lambda_{max}(P_{c2})\right] \| e_x(0)\|^2 \\ + \gamma_o^2 \left(\rho_2 + \rho_1 \gamma_c^2\right) \int_0^T \| \omega_x(t)\|^2 dt.\end{aligned} \tag{31}$$

According to Theorems 1 and 2, the design criteria of the H_∞ observer and controller based on the lateral dynamics model are established to ensure the robustness of path tracking.

5. Design of Feedforward Controller

How to obtain excellent performance in path tracking is a key technology for autonomous vehicles. Feedforward–feedback control architectures are suitable for accurate path tracking with adequate margins of stability [30]. Due to the inclusion of curvature c in the system model, the steady-state deviation when driving on a road with significant curvature is not 0 [31]. Feedforward control can provide an immediate response input to the steering wheel and suppress the static error of the system, so it is necessary to design the feedforward controller.

If the transmission ratio of the vehicle steering system is i, then

$$\delta = \frac{\delta_b + \delta_f}{i}, \tag{32}$$

where δ_f and δ_b are adaptive feedforward and feedback control of the steering wheel angle, respectively.

According to Equation (1), we can obtain

$$\dot{\tilde{X}} = \tilde{A}\tilde{X} + \tilde{B}_1 \frac{\delta_b}{i} + \tilde{B}_1 \frac{\delta_f}{i} + \tilde{B}_2 c. \tag{33}$$

It is obvious from Equation (33) that neither $\dot{e_1}$ nor $\dot{e_2}$ can be 0 simultaneously. In addition, the distance deviation e_1 is the primary concern for path tracking, and therefore the adaptive feedforward control is utilized to force the feedforward deviation of $\dot{e_1}$ to be 0. Then,

$$\frac{2C_{af}}{m}\frac{\delta_f}{i} - V_{ego}^2 c - \frac{2C_{af}l_f - 2C_{ar}l_r}{m} c = 0. \tag{34}$$

The adaptive feedforward of the controller is

$$\delta_f = \frac{mV_{ego}^2 + 2C_{af}l_f - 2C_{ar}l_r}{2C_{af}} ic, \tag{35}$$

which implies that adaptive feedforward is proportional to the path curvature. However, the experimental results illustrate that e_1 and e_2 of the controller with adaptive feedforward

are still proportional to the road curvature, which may be caused by model errors or measurement noise. Hence, an additional proportionate feedforward is considered to further reduce the errors, and the ideal steering wheel angle is

$$\begin{aligned}\delta_{wheel} &= \delta_b + \delta_f + \delta_k \\ &= K\hat{x}(t) + \frac{mV_{ego}^2 + 2C_{af}l_f - 2C_{ar}l_r}{2C_{af}}ic + K_p c,\end{aligned} \tag{36}$$

where δ_k is proportional feedforward, and K_p is the proportional feedforward coefficient, which can be calibrated by the experiments.

Remark 4. *The feedback control of the ideal steering wheel angle makes the system achieve dynamic stability to solve path tracking issues. However, the adjustment effect of feedback control lags behind the disturbance of road curvature. In order to improve the control accuracy, a compound control system is constructed with feedforward control as a supplement when the road curvature can be measured. The adaptive feedforward realizes the initial adjustment of curvature interference, and the proportional feedforward further improves the performance of path tracking by taking advantage of the conclusion that tracking error is proportional to road curvature.*

6. Experiment and Analysis

In this section, hardware-in-the-loop (HIL) tests are implemented to demonstrate the performance of the designed controller. The HIL platform offers the advantage of combining software systems with other system components for modeling or simulation, thereby enabling the acquisition of high-fidelity experimental results [32].

The HIL platform is constructed based on Dspace Micro Autobox II, which provides us with a convenient tool to build the control algorithm. The road scenario is set up by the host PC. Simultaneously, a smart camera is employed to acquire road information in order to imitate the real driving environment. All signals are transmitted via the CAN-bus, and the HIL platform is shown in Figure 3. The dynamics parameters of virtual vehicles are presented in Table 2.

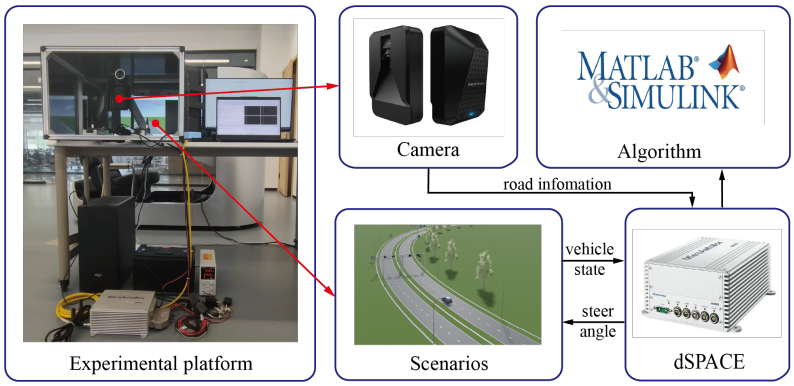

Figure 3. Schema of the HIL platform.

Table 2. Dynamic parameters of the virtual vehicle.

Description	Symbol	Parameters
Vehicle mass	m	1304 (kg)
Vehicle yaw moment of inertia	I_z	1500 (m/s^2)
Cornering stiffness of front/rear tires	C_{af}, C_{ar}	48,000, 44,000 (N/rad)
Distance from center of mass to front/rear axes	l_f, l_r	1.004, 1.480 (m)

In the design and analysis of controls for autonomous vehicles, the MPC control algorithm is a frequently utilized approach. The vehicle model used by the MPC algorithm is shown in Equation (1), and when it is discretized, the state space equation can be written as:

$$x(k+1) = (\tilde{A}T + I)x(k) + \tilde{B_1}Tu(k) + \tilde{B_2}Tc(k), \tag{37}$$

where T is the discrete sampling time, and I is the identity matrix of the appropriate dimension.

If Equation (37) is further transformed into a control increment, it can be rewritten as:

$$\xi(k+1) = \breve{A}\xi(k) + \breve{B_1}\Delta u(k) + \breve{B_2}c(k), \tag{38}$$

where

$$\xi(k+1) = \begin{bmatrix} x(k+1) \\ u(k) \end{bmatrix}, \breve{A} = \begin{bmatrix} \tilde{A}T + I & \tilde{B_1}T \\ 0 & I \end{bmatrix},$$
$$\breve{B_1} = \begin{bmatrix} \tilde{B_1}T \\ I \end{bmatrix}, \breve{B_2} = \begin{bmatrix} \tilde{B_2}T \\ 0 \end{bmatrix}, \Delta u(k) = u(k) - u(k-1).$$

The prediction time domain is set to N_p, the control time domain is set to N_c, and the output matrix is assigned as $\breve{C}$. Consequently, the output state variable of the MPC can be represented as:

$$Y = \Psi\xi(k) + \Xi\Delta u + \Gamma K, \tag{39}$$

where

$$Y = \begin{bmatrix} \eta(k+1) \\ \eta(k+2) \\ \cdots \\ \eta(k+N_c) \\ \cdots \\ \eta(k+N_p) \end{bmatrix} = \begin{bmatrix} \breve{C}\xi(k+1) \\ \breve{C}\xi(k+2) \\ \cdots \\ \breve{C}\xi(k+N_c) \\ \cdots \\ \breve{C}\xi(k+N_p) \end{bmatrix}, \Psi = \begin{bmatrix} \breve{C}\breve{A} \\ \breve{C}\breve{A}^2 \\ \cdots \\ \breve{C}\breve{A}^{N_c} \\ \cdots \\ \breve{C}\breve{A}^{N_p} \end{bmatrix}, \Delta u = \begin{bmatrix} \Delta u(k) \\ \Delta u(k+1) \\ \cdots \\ \Delta u(k+N_c-1) \end{bmatrix},$$

$$\Xi = \begin{bmatrix} \breve{C}\breve{B_1} & 0 & \cdots & 0 \\ \breve{C}\breve{A}\breve{B_1} & \breve{C}\breve{B_1} & \cdots & 0 \\ \cdots & \cdots & \ddots & \cdots \\ \breve{C}\breve{A}^{N_c-1}\breve{B_1} & \breve{C}\breve{A}^{N_c-2}\breve{B_1} & \cdots & \breve{C}\breve{B_1} \\ \cdots & \cdots & \cdots & \cdots \\ \breve{C}\breve{A}^{N_p-1}\breve{B_1} & \breve{C}\breve{A}^{N_p-2}\breve{B_1} & \cdots & \breve{C}\breve{A}^{N_p-N_c}\breve{B_1} \end{bmatrix}, K = \begin{bmatrix} c(k) \\ c(k+1) \\ \cdots \\ c(k+N_c-1) \end{bmatrix},$$

$$\Gamma = \begin{bmatrix} \breve{C}\breve{B_2} & 0 & \cdots & 0 \\ \breve{C}\breve{A}\breve{B_2} & \breve{C}\breve{B_2} & \cdots & 0 \\ \cdots & \cdots & \ddots & \cdots \\ \breve{C}\breve{A}^{N_c-1}\breve{B_2} & \breve{C}\breve{A}^{N_c-2}\breve{B_2} & \cdots & \breve{C}\breve{B_2} \\ \cdots & \cdots & \cdots & \cdots \\ \breve{C}\breve{A}^{N_p-1}\breve{B_2} & \breve{C}\breve{A}^{N_p-2}\breve{B_2} & \cdots & \breve{C}\breve{A}^{N_p-N_c}\breve{B_2} \end{bmatrix}, \breve{C} = \begin{bmatrix} 1 & 0 & 0 & 0 \\ 0 & 0 & 1 & 0 \end{bmatrix}.$$

The cost function of the MPC is described as follows:

$$J = \sum_{i=1}^{N_p} \left\| \eta(k+i) - \eta_{ref}(k+i) \right\|_Q^2 + \sum_{i=0}^{N_c-1} \|\Delta u(k+i)\|_R^2, \tag{40}$$

where Q and R are the weight coefficients for the predicted state variable and the control input increment, respectively.

In order to simplify the calculation, the road curvature in the future period of time is set as the current path curvature: $c(k) = c(k+1) = \cdots = c(k+N_c-1)$. The reference value of the system output is expressed as follows:

$$\begin{aligned} Y_{ref} &= [\eta_{ref}(k+1), \eta_{ref}(k+2), \cdots, \eta_{ref}(k+N_c), \cdots \eta_{ref}(k+N_p)]^T \\ &= [0, 0, \cdots, 0, \cdots, 0]^T. \end{aligned} \tag{41}$$

By comparing with the MPC control method, the proposed controller is validated.

It is worth noting that, in the context of MPC for path tracking, the system model takes into account the influence of road curvature, as demonstrated in Equation (37). When designing the H_∞ observer and controller, the impact of road curvature is treated as an external interference term. Therefore, to enhance vehicle path tracking performance, the feedforward control based on the road curvature term is incorporated into the H_∞ controller. Additionally, the design process of the H_∞ controller takes into consideration the dynamic characteristics of the steering actuator in order to ensure optimal control performance for the actual vehicle. However, in the actual hardware loop simulation, as depicted in Figure 3, there is only a communication delay between the controller and the host PC. Hence, for the MPC method, we disregard any delays caused by the steering system.

The feedback gain of the proposed method and the MPC control increment are calculated using parameters that do not match the vehicle model, as presented in Table 3. The parameter uncertainties are within the range of ±15% of the reference parameter value. On this basis, the longitudinal speed of the vehicle is divided into several unequal intervals, and the feedback gain of the H_∞ observer and H_∞ controller corresponding to each speed interval is calculated.

Table 3. Dynamic parameters that do not match the virtual vehicle.

Description	Symbol	Parameters
Vehicle mass	m	1400 (kg)
Vehicle yaw moment of inertia	I_z	1750 (m/s^2)
Cornering stiffness of front/rear tires	C_{af}, C_{ar}	52,000, 48,000 (N/rad)
Distance from center of mass to front/rear axes	l_f, l_r	1.100, 1.380 (m)

6.1. Test Scenario 1

Scenario 1 is used to verify the performance of the proposed controller on urban roads. The desired path is taken from real-world urban roads with complex curvature changes. The road curvature obtained by the smart camera is shown in Figure 4a, and the maximum curvature can reach about 0.044 m^{-1}.

Due to the influence of traffic lights and traffic flow on urban roads, the longitudinal speed of vehicles is time-varying and includes stop–go operating conditions. In the process of driving, the vehicle speed is not uniform in terms of acceleration and deceleration, as shown in Figure 4b.

The HIL experimental results of vehicle lateral distance error e_1 and heading error e_2 are shown in Figure 5a and Figure 5b, respectively. The lateral distance errors for the proposed control method and the MPC controller are bounded by ±0.1566 m and ±0.3283 m, and the heading errors of the two schemes are limited to within ±0.0573 rad and ±0.0711 rad. Furthermore, the lateral distance error and heading error regulated by the proposed approach are enhanced by 52.30% and 19.41% compared with the MPC controller, which indicates the proposed control system's tracking accuracy exceeds that of the MPC controller by a wide margin.

Notably, the variation trend in the lateral distance error and the heading error under the proposed control approach is approximately consistent with the desired path curvature. This indicates that the lateral distance error and heading error can be compensated for by the feedforward control combined with road curvature information. Therefore, the proportional term of curvature is added on the basis of adaptive feedforward.

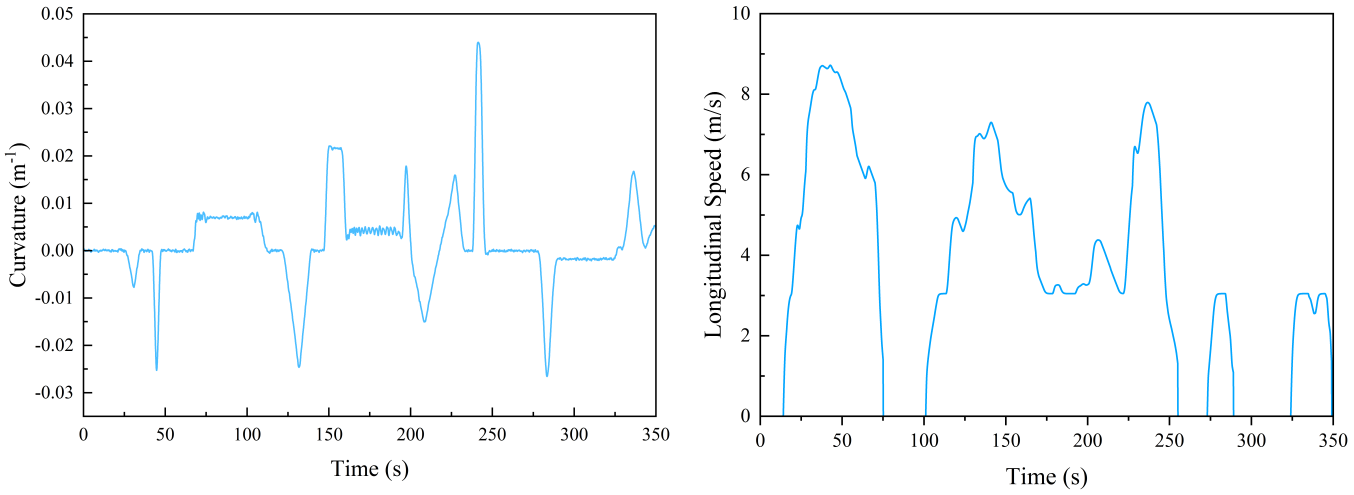

(a) Road curvature (b) Longitudinal speed

Figure 4. Road curvature and longitudinal speed in an urban scenario.

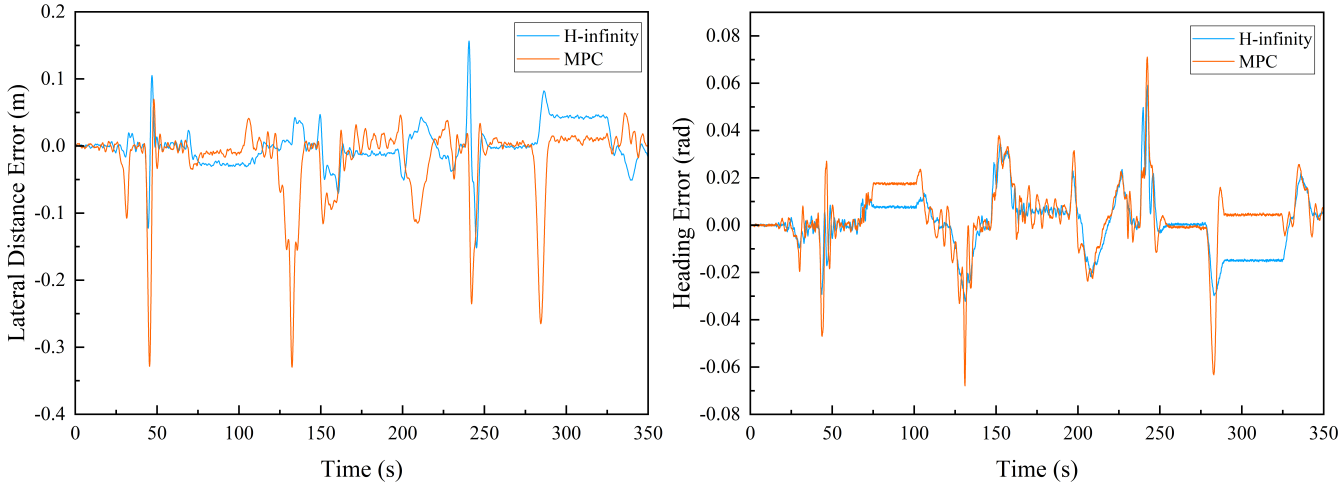

(a) Lateral distance error (b) Heading error

Figure 5. Comparison of tracking errors between the H_∞ and MPC control methods in an urban scenario.

It can be shown from a comparison of the lateral distance errors and heading errors under the proposed control scheme and MPC control methods that the two errors controlled by the MPC exhibit clear oscillations when the desired path curvature changes and that it takes some time to return to the steady state.

A comparison of the yaw rate obtained by the proposed approach and the MPC controller is shown in Figure 6a. The yaw rate's amount indicates the vehicle's security and stability, and its variation has an impact on how comfortable it is. Figure 6b illustrates that the yaw rate obtained by the proposed control scheme is smoother than that of the MPC. In addition, the detrended fluctuation analysis is a method used to eliminate the trend components of the intrinsic properties and to reveal the fluctuations of the system. The standard deviation of the yaw rate detrended fluctuation data of the proposed control strategy and the MPC controller are 0.0067 rad/s and 0.0094 rad/s respectively. The former is improved by 28.72% over the latter, which indicates that the vehicle controlled by the proposed control approach possesses superior comfort when turning.

In summary, the proposed method can achieve excellent tracking results in urban road scenarios, and the comfort and safety of path tracking can be guaranteed.

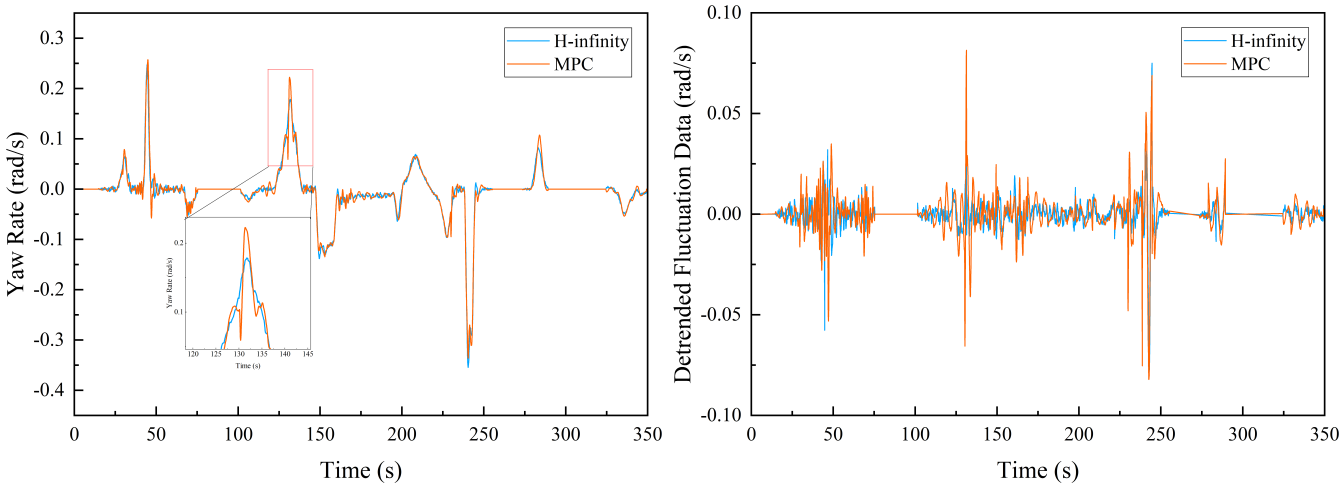

(a) Yaw rate (b) Detrended fluctuation data

Figure 6. Comparison of yaw rate and detrended fluctuation data between the H_∞ and MPC control methods in an urban scenario.

6.2. Test Scenario 2

In order to further verify the performance and robustness of the designed controller at higher vehicle speeds, a second scenario is adopted.

The road curvature of the highway scene obtained by the camera is shown in Figure 7a. The autonomous vehicle must pass through five gently changing arc roads with a maximum curvature of -0.0013 m^{-1}. The actual speed of the vehicle is depicted in Figure 7b, which includes most of the speed of the real vehicle when driving on the highway, and the maximum velocity is 30.84 m/s.

The lateral distance errors and heading errors of the vehicle in the highway scenario are demonstrated in Figure 8a and Figure 8b, respectively. The lateral distance errors of the proposed control scheme and the MPC controller are restricted by ± 0.1772 m and ± 0.2406 m, and the heading errors of the two methods are bounded within ± 0.0041 deg and ± 0.0048 deg. Compared with the MPC controller, the lateral distance error and heading error of the proposed control strategy are improved by 26.35% and 14.58%, respectively. As can be seen, the proposed control method has a superior tracking effect compared to the MPC control.

The lateral distance error and heading error under the proposed control method change with the varying trend of road curvature. However, the extreme point's size of error in a highway scenario does not exactly match the curvature value. Obviously, the vehicle speed is also a factor in the lateral distance error and the heading error, in addition to the road's curvature. Therefore, even though the tracking errors are within the acceptable range, it is more logical to take into account both velocity and road curvature in the feedforward control in a highway scenario.

The change rate of the path curvature is also correlated with the gradient of the heading error under the proposed control approach. The absolute value of the heading error slope will also increase when the change rate of the curvature is sudden. As seen in Figure 8b, when the path curvature changes abruptly, the heading error controlled by the proposed control approach fluctuates significantly.

The result of the yaw rate is shown in Figure 9a. Compared with the MPC controller, the yaw rate of the proposed control scheme has not strongly oscillated. The standard deviation of the yaw rate detrended fluctuation data of the proposed control strategy and the MPC controller are 0.0002 rad/s and 0.0010 rad/s, respectively, which indicates that the proposed control scheme can still show better comfort at high vehicle speeds.

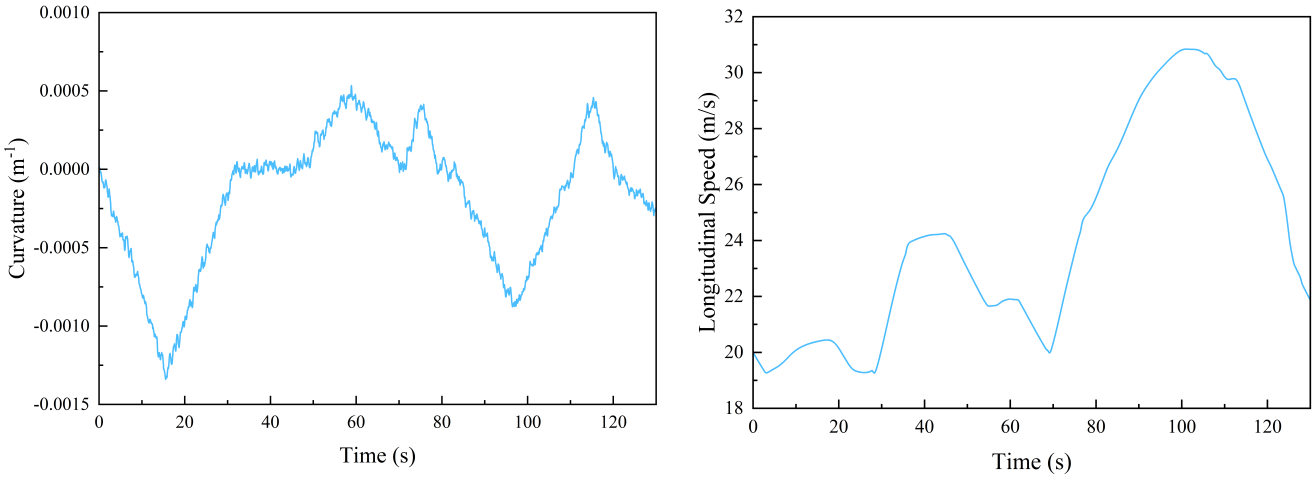

(a) Road curvature (b) Longitudinal speed

Figure 7. Road curvature and longitudinal speed in a highway scenario.

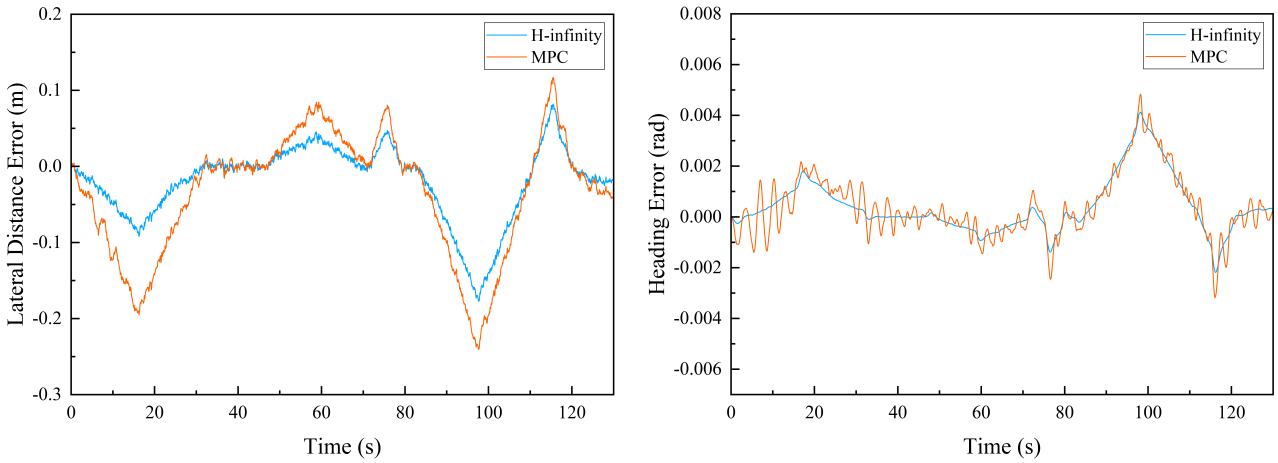

(a) Lateral distance error (b) Heading error

Figure 8. Comparison of tracking errors between the H_∞ and MPC control methods in a highway scenario.

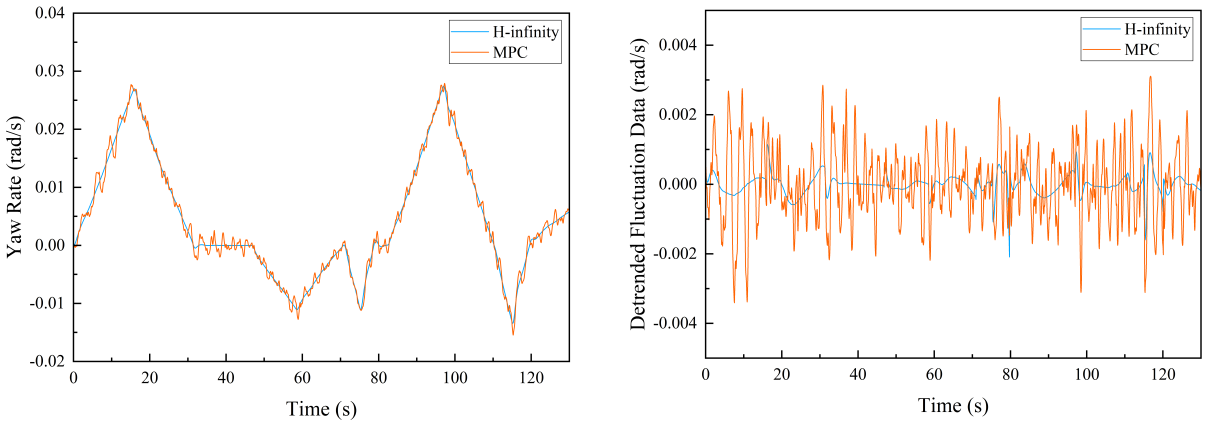

(a) Yaw rate (b) Detrended fluctuation data

Figure 9. Comparison of yaw rate and detrended fluctuation data between the H_∞ and MPC control methods in a highway scenario.

In conclusion, compared with the MPC control, which is an optimization control strategy, the proposed control approach effectively improves the accuracy of path tracking, assuring vehicle safety while also taking driver comfort into consideration, as shown in Table 4. Meanwhile, the real-time performance of the proposed method is verified by HIL experiments. In addition, the experiment includes urban and highway scenarios, so it can be applied in practice. It should be emphasized that the proposed control approach can be applied as a generic technique for lane-keeping assistance and lane changing, in addition to path tracking.

Table 4. Tracking performance.

Scenarios	Indicators	H-Infinity	MPC	Improved
Urban	$max\|e_1\|$	0.1566	0.3283	52.30%
	$max\|e_2\|$	0.0573	0.0711	19.41%
	$\sigma(DF(\dot{\psi}))$	0.0067	0.0094	28.72%
Highway	$max\|e_1\|$	0.1772	0.2406	26.35%
	$max\|e_2\|$	0.0041	0.0048	14.58%
	$\sigma(DF(\dot{\psi}))$	0.0002	0.0010	80.00%

Note that $max|\cdot|$ denotes the maximum of the absolute value, $DF(\cdot)$ indicates the detrended fluctuation data, and $\sigma(\cdot)$ represents the standard deviation.

7. Conclusions

A robust lateral control strategy with a state observer is proposed to improve the path tracking performance of the vehicle. Firstly, the uncertainty of all parameters is considered in the dynamic model design. Furthermore, in order to achieve state feedback and enhance system performance, the design criteria of the H_∞ observer and controller are established based on the LMI technique, and a feedforward controller is designed to further reduce the tracking error. Finally, the effectiveness of the proposed controller in an urban road scene and a highway scene is verified by HIL simulation experiments. The experimental results demonstrate that, in comparison with the traditional MPC method, the proposed control approach exhibits superior tracking accuracy and reduced fluctuation. Although the results of the HIL simulation provide valuable guidance for practical applications, the performance of the proposed controller in a real vehicle holds paramount importance. Hence, the influence between the controller and the actual vehicle should be given special attention in future research endeavors to further enhance vehicle performance.

Author Contributions: Conceptualization and methodology, J.W. and C.L.; validation and writing, J.W. and B.W.; review and editing, L.Z. and L.L. All authors have read and agreed to the published version of the manuscript.

Funding: This research was funded by the National Science Fund of the People's Republic of China (grant number: 52102444), the Open Fund of the State Key Laboratory of Automotive Safety and Energy of Tsinghua University (grant number: KFY2205), and the Central Guidance on Local Science and Technology Development Fund of Hebei Province (grant number: 226Z2204G).

Data Availability Statement: The original contributions presented in the study are included in the article, further inquiries can be directed to the corresponding author.

Conflicts of Interest: The authors declare no conflicts of interest.

Appendix A

$$\begin{aligned}
\frac{C_{af}+C_{ar}}{mV_{ego}} &= \left[\left(C_{fe}+N(t)\bar{C}_{fn}\right)+\left(C_{re}+N(t)\bar{C}_{rn}\right)\right]\left(m_e+N(t)\bar{m}_n\right)\left(V_e+N(t)\bar{V}_n\right)\\
&= \left[\left(C_{fe}+C_{re}\right)+\left(\bar{C}_{fn}+\bar{C}_{rn}\right)N(t)\right]\left[m_eV_e+\left(m_e\bar{V}_n+V_e\bar{m}_n\right)N(t)+\bar{m}_n\bar{V}_nN^2(t)\right]\\
&= \left(C_{fe}+C_{re}\right)m_eV_e+\left[\left(C_{fe}+C_{re}\right)\left(m_e\bar{V}_n+V_e\bar{m}_n\right)+\left(\bar{C}_{fn}+\bar{C}_{rn}\right)m_eV_e\right]N(t)\\
&\quad+\left[\left(C_{fe}+C_{re}\right)\bar{m}_n\bar{V}_n+\left(\bar{C}_{fn}+\bar{C}_{rn}\right)\left(m_e\bar{V}_n+V_e\bar{m}_n\right)\right]N^2(t)\\
&\quad+\left(\bar{C}_{fn}+\bar{C}_{rn}\right)\bar{m}_n\bar{V}_nN^3(t)\\
\frac{C_{af}+C_{ar}}{m} &= \left[\left(C_{fe}+N(t)\bar{C}_{fn}\right)+\left(C_{re}+N(t)\bar{C}_{rn}\right)\right]\left(m_e+N(t)\bar{m}_n\right)\\
&= \left(C_{fe}+C_{re}\right)m_e+\left[\left(C_{fe}+C_{re}\right)\bar{m}_n+\left(\bar{C}_{fn}+\bar{C}_{rn}\right)m_e\right]N(t)\\
&\quad+\left(\bar{C}_{fn}+\bar{C}_{rn}\right)\bar{m}_nN^2(t)\\
\frac{C_{\mathrm{af}}l_f-C_{\mathrm{ar}}l_r}{mV_{ego}} &= \left[\left(C_{fe}+N(t)\bar{C}_{fn}\right)\left(l_{fe}+N(t)\bar{l}_{fn}\right)-\left(C_{re}+N(t)\bar{C}_{rn}\right)\left(l_{re}+N(t)\bar{l}_{rn}\right)\right]\\
&\quad\left[\left(m_e+N(t)\bar{m}_n\right)\left(V_e+N(t)\bar{V}_n\right)\right]\\
&= \left(C_{fe}+N(t)\bar{C}_{fn}\right)\left(l_{fe}+N(t)\bar{l}_{fn}\right)m_eV_e+\left(C_{fe}+N(t)\bar{C}_{fn}\right)\left(l_{fe}+N(t)\bar{l}_{fn}\right)\\
&\quad\left[\left(m_e\bar{V}_n+V_e\bar{m}_n\right)N(t)+\bar{m}_n\bar{V}_nN^2(t)\right]-\left(C_{re}+N(t)\bar{C}_{rn}\right)\left(l_{re}+N(t)\bar{l}_{rn}\right)m_eV_e\\
&\quad-\left(C_{re}+N(t)\bar{C}_{rn}\right)\left(l_{re}+N(t)\bar{l}_{rn}\right)\left[\left(m_e\bar{V}_n+V_e\bar{m}_n\right)N(t)+\bar{m}_n\bar{V}_nN^2(t)\right]\\
&= \left(C_{fe}l_{fe}-C_{re}l_{re}\right)m_eV_e+\left[\left(C_{fe}\bar{l}_{fn}+l_{fe}\bar{C}_{fn}-C_{re}\bar{l}_{rn}-l_{re}\bar{C}_{rn}\right)m_eV_e\right.\\
&\quad\left.+\left(C_{fe}l_{fe}-C_{re}l_{re}\right)\left(m_e\bar{V}_n+V_e\bar{m}_n\right)\right]N(t)+\left[\left(\bar{C}_{fn}\bar{l}_{fn}-\bar{C}_{rn}\bar{l}_{rn}\right)m_eV_e\right.\\
&\quad\left.+\left(C_{fe}\bar{l}_{fn}+l_{fe}\bar{C}_{fn}-C_{re}\bar{l}_{rn}-l_{re}\bar{C}_{rn}\right)\left(m_e\bar{V}_n+V_e\bar{m}_n\right)+\left(C_{fe}l_{fe}-C_{re}l_{re}\right)\bar{m}_n\bar{V}_n\right]\\
&\quad N^2(t)+\left[\left(\bar{C}_{fn}\bar{l}_{fn}-\bar{C}_{rn}\bar{l}_{rn}\right)\left(m_e\bar{V}_n+V_e\bar{m}_n\right)+\left(C_{fe}\bar{l}_{fn}+l_{fe}\bar{C}_{fn}-C_{re}\bar{l}_{rn}-l_{re}\bar{C}_{rn}\right)\right.\\
&\quad\left.\bar{m}_n\bar{V}_n\right]N^3(t)+\left(\bar{C}_{fn}\bar{l}_{fn}-\bar{C}_{rn}\bar{l}_{rn}\right)\bar{m}_n\bar{V}_nN^4(t)\\
\frac{C_{\mathrm{af}}l_f-C_{\mathrm{ar}}l_r}{I_{\mathrm{z}}V_{ego}} &= \left[\left(C_{fe}+N(t)\bar{C}_{fn}\right)\left(l_{fe}+N(t)\bar{l}_{fn}\right)-\left(C_{re}+N(t)\bar{C}_{rn}\right)\left(l_{re}+N(t)\bar{l}_{rn}\right)\right]\\
&\quad\left[\left(I_e+N(t)\bar{I}_n\right)\left(V_e+N(t)\bar{V}_n\right)\right]\\
&= \left(C_{fe}+N(t)\bar{C}_{fn}\right)\left(l_{fe}+N(t)\bar{l}_{fn}\right)I_eV_e+\left(C_{fe}+N(t)\bar{C}_{fn}\right)\left(l_{fe}+N(t)\bar{l}_{fn}\right)\\
&\quad\left[\left(I_e\bar{V}_n+V_e\bar{I}_n\right)N(t)+\bar{I}_n\bar{V}_nN^2(t)\right]-\left(C_{re}+N(t)\bar{C}_{rn}\right)\left(l_{re}+N(t)\bar{l}_{rn}\right)I_eV_e\\
&\quad-\left(C_{re}+N(t)\bar{C}_{rn}\right)\left(l_{re}+N(t)\bar{l}_{rn}\right)\left[\left(I_e\bar{V}_n+V_e\bar{I}_n\right)N(t)+\bar{I}_n\bar{V}_nN^2(t)\right]
\end{aligned}$$

$$
\begin{aligned}
&= \left(C_{fe}l_{fe} - C_{re}l_{re}\right)I_eV_e + \left[\left(C_{fe}\bar{I}_{fn} + l_{fe}\bar{C}_{fn} - C_{re}\bar{I}_{rn} - l_{re}\bar{C}_{rn}\right)I_eV_e + \left(C_{fe}l_{fe} - C_{re}l_{re}\right)\right.\\
&\left.(I_e\bar{V}_n + V_e\bar{I}_n)\right]N(t) + \left[\left(\bar{C}_{fn}\bar{I}_{fn} - \bar{C}_{rn}\bar{I}_{rn}\right)I_eV_e + \left(C_{fe}\bar{I}_{fn} + l_{fe}\bar{C}_{fn} - C_{re}\bar{I}_{rn} - l_{re}\bar{C}_{rn}\right)\right.\\
&\left.(I_e\bar{V}_n + V_e\bar{I}_n) + \left(C_{fe}l_{fe} - C_{re}l_{re}\right)\bar{I}_n\bar{V}_n\right]N^2(t) + \left[\left(\bar{C}_{fn}\bar{I}_{fn} - \bar{C}_{rn}\bar{I}_{rn}\right)(I_e\bar{V}_n + V_e\bar{I}_n)\right.\\
&\left.+\left(C_{fe}\bar{I}_{fn} + l_{fe}\bar{C}_{fn} - C_{re}\bar{I}_{rn} - l_{re}\bar{C}_{rn}\right)\bar{I}_n\bar{V}_n\right]N^3(t) + \left(\bar{C}_{fn}\bar{I}_{fn} - \bar{C}_{rn}\bar{I}_{rn}\right)\bar{I}_n\bar{V}_nN^4(t)
\end{aligned}
$$

$$
\begin{aligned}
\frac{C_{\mathrm{af}}l_f - C_{\mathrm{ar}}l_r}{I_z} &= \left[\left(C_{fe} + N(t)\bar{C}_{fn}\right)\left(l_{fe} + N(t)\bar{l}_{fn}\right) - (C_{re} + N(t)\bar{C}_{rn})\left(l_{re} + N(t)\bar{l}_{rn}\right)\right](I_e + N(t)\bar{I}_n)\\
&= \left(C_{fe} + N(t)\bar{C}_{fn}\right)\left(l_{fe} + N(t)\bar{l}_{fn}\right)I_e + \left(C_{fe} + N(t)\bar{C}_{fn}\right)\left(l_{fe} + N(t)\bar{l}_{fn}\right)N(t)\bar{I}_n\\
&\quad - (C_{re} + N(t)\bar{C}_{rn})\left(l_{re} + N(t)\bar{l}_{rn}\right)I_e - (C_{re} + N(t)\bar{C}_{rn})\left(l_{re} + N(t)\bar{l}_{rn}\right)N(t)\bar{I}_n\\
&= \left(C_{fe}l_{fe} - C_{re}l_{re}\right)I_e + \left[\left(C_{fe}\bar{I}_{fn} + l_{fe}\bar{C}_{fn} - C_{re}\bar{I}_{rn} - l_{re}\bar{C}_{rn}\right)I_e + \left(C_{fe}l_{fe} - C_{re}l_{re}\right)\bar{I}_n\right]\\
&\quad N(t) + \left[\left(\bar{C}_{fn}\bar{I}_{fn} - \bar{C}_{rn}\bar{I}_{rn}\right)I_e + \left(C_{fe}\bar{I}_{fn} + l_{fe}\bar{C}_{fn} - C_{re}\bar{I}_{rn} - l_{re}\bar{C}_{rn}\right)\bar{I}_n\right]N^2(t)\\
&\quad + \left(\bar{C}_{fn}\bar{I}_{fn} - \bar{C}_{rn}\bar{I}_{rn}\right)\bar{I}_nN^3(t)
\end{aligned}
$$

$$
\begin{aligned}
\frac{C_{\mathrm{af}}l_f^2 + C_{\mathrm{ar}}l_r^2}{I_zV_{ego}} &= \left[\left(C_{fe} + N(t)\bar{C}_{fn}\right)\left(l_{fe} + N(t)\bar{l}_{fn}\right)^2 + (C_{re} + N(t)\bar{C}_{rn})\left(l_{re} + N(t)\bar{l}_{rn}\right)^2\right]\\
&\quad [(I_e + N(t)\bar{I}_n)(V_e + N(t)\bar{V}_n)]\\
&= \left(C_{fe} + N(t)\bar{C}_{fn}\right)\left(l_{fe}^2 + 2l_{fe}\bar{l}_{fn}N(t) + \bar{l}_{fn}^2N^2(t)\right)[I_eV_e + (I_e\bar{V}_n + V_e\bar{I}_n)N(t)\\
&\quad + \bar{I}_n\bar{V}_nN^2(t)\Big] + (C_{re} + N(t)\bar{C}_{rn})\left(l_{re}^2 + 2l_{re}\bar{l}_{rn}N(t) + \bar{l}_{rn}^2N^2(t)\right)[I_eV_e + (I_e\bar{V}_n + V_e\bar{I}_n)\\
&\quad N(t) + \bar{I}_n\bar{V}_nN^2(t)\Big]\\
&= \left(C_{fe}l_{fe}^2 + C_{re}l_{re}^2\right)I_eV_e + \left[\left(2C_{fe}l_{fe}\bar{l}_{fn} + 2C_{re}l_{re}\bar{l}_{rn} + \bar{C}_{fn}l_{fe}^2 + \bar{C}_{rn}l_{re}^2\right)I_eV_e + \left(C_{fe}l_{fe}^2\right.\right.\\
&\quad \left.\left.+C_{re}l_{re}^2\right)(I_e\bar{V}_n + V_e\bar{I}_n)\right]N(t) + \left[\left(C_{fe}\bar{l}_{fn}^2 + C_{re}\bar{l}_{rn}^2 + 2\bar{C}_{fn}\bar{l}_{fn}l_{fe} + 2\bar{C}_{rn}\bar{l}_{rn}l_{re}\right)I_eV_e\right.\\
&\quad \left.+\left(\bar{C}_{fn}l_{fe}^2 + \bar{C}_{rn}l_{re}^2 + 2C_{fe}l_{fe}\bar{l}_{fn} + 2C_{re}l_{re}\bar{l}_{rn}\right)(I_e\bar{V}_n + V_e\bar{I}_n) + \left(C_{fe}l_{fe}^2 + C_{re}l_{re}^2\right)\bar{I}_n\bar{V}_n\right]\\
&\quad N^2(t) + \left[\left(\bar{C}_{fn}\bar{l}_{fn}^2 + \bar{C}_{rn}\bar{l}_{rn}^2\right)I_eV_e + \left(C_{fe}\bar{l}_{fn}^2 + C_{re}\bar{l}_{rn}^2 + 2\bar{C}_{fn}\bar{l}_{fn}l_{fe} + 2\bar{C}_{rn}\bar{l}_{rn}l_{re}\right)(I_e\bar{V}_n\right.\\
&\quad \left.+V_e\bar{I}_n) + \left(2C_{fe}l_{fe}\bar{l}_{fn} + 2C_{re}l_{re}\bar{l}_{rn} + \bar{C}_{fn}l_{fe}^2 + \bar{C}_{rn}l_{re}^2\right)\bar{I}_n\bar{V}_n\right]N^3(t) + \left[\left(\bar{C}_{fn}\bar{l}_{fn}^2\right.\right.\\
&\quad \left.\left.+\bar{C}_{rn}\bar{l}_{rn}^2\right)(I_e\bar{V}_n + V_e\bar{I}_n) + \left(C_{fe}\bar{l}_{fn}^2 + C_{re}\bar{l}_{rn}^2 + 2\bar{C}_{fn}\bar{l}_{fn}l_{fe} + 2\bar{C}_{rn}\bar{l}_{rn}l_{re}\right)\bar{I}_n\bar{V}_n\right]N^4(t)\\
&\quad + \left(\bar{C}_{fn}\bar{l}_{fn}^2 + \bar{C}_{rn}\bar{l}_{rn}^2\right)\bar{I}_n\bar{V}_nN^5(t)
\end{aligned}
$$

$$
\begin{aligned}
\frac{C_{af}}{m} &= \left(C_{fe} + N(t)\bar{C}_{fn}\right)(m_e + N(t)\bar{m}_n) = C_{fe}m_e + \left(C_{fe}\bar{m}_n + \bar{C}_{fn}m_e\right)N(t) + \bar{C}_{fn}\bar{m}_nN^2(t)\\
\frac{C_{\mathrm{af}}l_f}{I_z} &= \left(C_{fe} + N(t)\bar{C}_{fn}\right)\left(l_{fe} + N(t)\bar{l}_{fn}\right)(I_e + N(t)\bar{I}_n)\\
&= C_{fe}l_{fe}I_e + \left[\left(C_{fe}\bar{I}_{fn} + l_{fe}\bar{C}_{fn}\right)I_e + C_{fe}l_{fe}\bar{I}_n\right]N(t) + \left[\bar{C}_{fn}\bar{I}_{fn}I_e + \left(C_{fe}\bar{I}_{fn} + l_{fe}\bar{C}_{fn}\right)\bar{I}_n\right]\\
&\quad N^2(t) + \bar{C}_{fn}\bar{I}_{fn}\bar{I}_nN^3(t)
\end{aligned}
$$

$$
\begin{aligned}
V_{ego}^2 + \frac{2C_{af}l_f - 2C_{ar}l_r}{m} &= (V_{moe} + N(t)\bar{V}_{mon})^2 + 2\Big[\Big(C_{fe} + N(t)\bar{C}_{fn}\Big)\Big(l_{fe} + N(t)\bar{l}_{fn}\Big) \\
&\quad - (C_{re} + N(t)\bar{C}_{rn})\,(l_{re} + N(t)\bar{l}_{rn})\Big](m_e + N(t)\bar{m}_n) \\
&= {V_{moe}}^2 + 2\Big(C_{fe}l_{fe} - C_{re}l_{re}\Big)m_e + 2\Big[\Big(C_{fe}\bar{l}_{fn} + l_{fe}\bar{C}_{fn} - C_{re}\bar{l}_{rn} - l_{re}\bar{C}_{rn}\Big)m_e \\
&\quad + \Big(C_{fe}l_{fe} - C_{re}l_{re}\Big)\bar{m}_n + V_{moe}\bar{V}_{mon}\Big]N(t) + 2\Big[\Big(\bar{C}_{fn}\bar{l}_{fn} - \bar{C}_{rn}\bar{l}_{rn}\Big)m_e \\
&\quad + \Big(C_{fe}\bar{l}_{fn} + l_{fe}\bar{C}_{fn} - C_{re}\bar{l}_{rn} - l_{re}\bar{C}_{rn}\Big)\bar{m}_n + \frac{1}{2}\bar{V}_{mon}^2\Big]N^2(t) \\
&\quad + 2\Big(\bar{C}_{fn}\bar{l}_{fn} - \bar{C}_{rn}\bar{l}_{rn}\Big)\bar{m}_n N^3(t) \\
\frac{C_{\mathrm{af}}l_f^2 + C_{\mathrm{ar}}l_r^2}{I_z V_{ego}} &= \Big[\Big(C_{fe} + N(t)\bar{C}_{fn}\Big)\Big(l_{fe} + N(t)\bar{l}_{fn}\Big)^2 + (C_{re} + N(t)\bar{C}_{rn}) \\
&\quad (l_{re} + N(t)\bar{l}_{rn})^2\Big](I_e + N(t)\bar{I}_n) \\
&= \Big(C_{fe}l_{fe}^2 + C_{re}l_{re}^2\Big)I_e + \Big[\Big(2C_{fe}l_{fe}\bar{l}_{fn} + 2C_{re}l_{re}\bar{l}_{rn} + l_{fe}^2\bar{l}_{fn} + l_{re}^2\bar{l}_{rn}\Big)I_e \\
&\quad + \Big(C_{fe}l_{fe}^2 + C_{re}l_{re}^2\Big)\bar{I}_n\Big]N(t) + \Big[\Big(2l_{fe}\bar{l}_{fn}\bar{C}_{fn} + 2l_{re}\bar{l}_{rn}\bar{C}_{rn} + C_{fe}\bar{l}_{fn} + C_{re}\bar{l}_{rn}\Big)I_e \\
&\quad + \Big(2C_{fe}l_{fe}\bar{l}_{fn} + 2C_{re}l_{re}\bar{l}_{rn} + l_{fe}^2\bar{C}_{fn} + l_{re}^2\bar{C}_{rn}\Big)\bar{I}_n\Big]N^2(t) + \Big[\Big(\bar{C}_{fn}\bar{l}_{fn} \\
&\quad + \bar{C}_{rn}\bar{l}_{rn}\Big)I_e + \Big(C_{fe}\bar{l}_{fn} + C_{re}\bar{l}_{rn} + 2l_{fe}\bar{l}_{fn}\bar{C}_{fn} + 2l_{re}\bar{l}_{rn}\bar{C}_{rn}\Big)\bar{I}_n\Big]N^3(t) \\
&\quad + \Big[\Big(\bar{C}_{fn}\bar{l}_{fn} + \bar{C}_{rn}\bar{l}_{rn}\Big)\bar{I}_n\Big]N^4(t)
\end{aligned}
$$

References

1. Wang C.; Heng B.; Zhao W. Yaw and lateral stability control for four-wheel-independent steering and four-wheel-independent driving electric vehicle. *Proc. Inst. Mech. Eng. Part D J. Automob. Eng.* **2020**, *234*, 409–422. [CrossRef]
2. Zhang, H.; Lin, Y.; Han, S.; Lv, K. Lexicographic Actor-Critic Deep Reinforcement Learning for Urban Autonomous Driving. *IEEE Trans. Veh. Technol.* **2023**, *72*, 4308–4319. [CrossRef]
3. Fagnant, D. J.; Kockelman, K. Preparing a nation for autonomous vehicles: Opportunities, barriers and policy recommendations. *Transp. Res. Part A Policy Pract.* **2015**, *77*, 167–181. [CrossRef]
4. Jiang, J.; Astolfi, A. Lateral control of an autonomous vehicle. *IEEE Trans. Intell. Veh.* **2018**, *3*, 228–237. [CrossRef]
5. Attia, R.; Orjuela, R.; Basset, M. Combined longitudinal and lateral control for automated vehicle guidance. *Veh. Syst. Dyn.* **2014**, *52*, 261–279. [CrossRef]
6. Marino, R.; Scalzi, S.; Netto, M. Nested PID steering control for lane keeping in autonomous vehicles. *Control Eng. Pract.* **2011**, *19*, 1459–1467. [CrossRef]
7. Wang, X.; Fu, M.; Ma, H.; Yang, Y. Lateral control of autonomous vehicles based on fuzzy logic. *Control Eng. Pract.* **2015**, *34*, 1–17. [CrossRef]
8. Zhang, J.; Wang, H.; Zheng, J.; Cao, Z.; Man, Z.; Yu, M.; Chen, L. Adaptive sliding mode-based lateral stability control of steer-by-wire vehicles with experimental validations. *IEEE Trans. Veh. Technol.* **2020**, *69*, 9589–9600. [CrossRef]
9. Yang, T.; Bai, Z.; Li, Z.; Feng, N.; Chen, L. Intelligent Vehicle Lateral Control Method Based on Feedforward + Predictive LQR Algorithm. *Actuators* **2021**, *10*, 228. [CrossRef]
10. Ji, J.; Khajepour, A.; Melek, W. W.; Huang, Y. Path planning and tracking for vehicle collision avoidance based on model predictive control with multiconstraints. *IEEE Trans. Veh. Technol.* **2016**, *66*, 952–964. [CrossRef]
11. Wang, R.; Zhang, H.; Wang, J.; Yan, F.; Chen, N. Robust lateral motion control of four-wheel independently actuated electric vehicles with tire force saturation consideration. *J. Frankl. Inst.* **2015**, *2*, 645–668. [CrossRef]
12. Zhang, C.; Chu, D.; Liu, S.; Deng, Z.; Wu, C.; Su, X. Trajectory planning and tracking for autonomous vehicle based on state lattice and model predictive control. *IEEE Intell. Transp. Syst. Mag.* **2019**, *11*, 29–41. [CrossRef]
13. Liu, C. Z.; Li, L.; Chen, X.; Yong, J. W.; Cheng, S.; Dong, H. L. An Innovative Adaptive Cruise Control Method Based on Mixed H_2/H_∞ Out-of-Sequence Measurement Observer. *IEEE Trans. Intell. Transp. Syst.* **2021**, *23*, 5602–5614. [CrossRef]
14. Ni, J.; Hu, J.; Xiang, C. Robust path following control at driving/handling limits of an autonomous electric racecar. *IEEE Trans. Veh. Technol.* **2019**, *68*, 5518–5526. [CrossRef]
15. Wang, H.; Zhang, T.; Zhang, X.; Li, Q. Observer-based path tracking controller design for autonomous ground vehicles with input saturation. *IEEE/CAA J. Autom. Sin.* **2023**, *10*, 749–761. [CrossRef]
16. Hu, C.; Jing, H.; Wang, R.; Yan, F.; Chadli, M. Robust H_∞ output-feedback control for path following of autonomous ground vehicles. *Mech. Syst. Signal Process.* **2016**, *70*, 414–427. [CrossRef]

17. Guo, J.; Wang, J.; Luo, Y.; Li, K. Robust lateral control of autonomous four-wheel independent drive electric vehicles considering the roll effects and actuator faults. *Mech. Syst. Signal Process.* **2020**, *143*, 106773. [CrossRef]
18. Hang, P.; Chen, X.; Luo, F. LPV/H_∞ controller design for path tracking of autonomous ground vehicles through four-wheel steering and direct yaw-moment control. *Int. J. Automot. Technol.* **2019**, *20*, 679–691. [CrossRef]
19. Wang, R.; Jing, H.; Wang, J.; Chadli, M.; Chen, N. Robust output-feedback based vehicle lateral motion control considering network-induced delay and tire force saturation. *Neurocomputing* **2016**, *100*, 409–419. [CrossRef]
20. Guo, J.; Luo, Y.; Li, K. Robust H_∞ fault-tolerant lateral control of four-wheel-steering autonomous vehicles. *Int. J. Automot. Technol.* **2020**, *21*, 993–1000. [CrossRef]
21. Li, C.; Jing, H.; Wang, R.; Chen, N. Vehicle lateral motion regulation under unreliable communication links based on robust H_∞ output-feedback control schema. *Mech. Syst. Signal Process.* **2018**, *104*, 171–187. [CrossRef]
22. Huang, X.; Zhang, H.; Zhang, G.; Wang, J. Robust Weighted Gain-Scheduling H_∞ Vehicle Lateral Motion Control With Considerations of Steering System Backlash-Type Hysteresis. *IEEE Trans. Control Syst. Technol.* **2014**, *22*, 1740–1753. [CrossRef]
23. Pang, H.; Liu, N.; Hu, C.; Xu, Z. A practical trajectory tracking control of autonomous vehicles using linear time-varying MPC method. *Proc. Inst. Mech. Eng. Part D J. Automob. Eng.* **2022**, *236*, 709–723. [CrossRef]
24. Hang, P.; Chen, X. Path tracking control of 4-wheel-steering autonomous ground vehicles based on linear parameter-varying system with experimental verification. *Proc. Inst. Mech. Eng. Part I J. Syst. Control Eng.* **2021**, *235*, 411–423. [CrossRef]
25. Jin, X. J.; Yin, G.; Chen, N. Gain-scheduled robust control for lateral stability of four-wheel-independent-drive electric vehicles via linear parameter-varying technique. *Mechatronics* **2015**, *30*, 286–296. [CrossRef]
26. Zhang, L.; Liu, C.; Wang, B.; Chen, X. An innovative method for scene recognition and target tracking for adaptive cruise control in complex traffic environment. *Proc. Inst. Mech. Eng. Part D J. Automob. Eng.* **2023**, *238*, 09544070231156956. [CrossRef]
27. Weng, C.; Cheng, W. Optimal tracking design with robust observer optimization. In Proceedings of the 2020 39th Chinese Control Conference (CCC), Shenyang, China, 27–29 July 2020; pp. 1837–1842.
28. Zhang, Z.; Zhang, N.; Huang, C.; Liu, X.; Ding, F. Observer-based H_∞ control for vehicle handling and stability subject to parameter uncertainties. *Proc. Inst. Mech. Eng. Part I J. Syst. Control Eng.* **2013**, *227*, 704–717. [CrossRef]
29. Sakthivel, R.; Arunkumar, A.; Mathiyalagan, K. Robust sampled-data H_∞ control for mechanical systems. *Complexity* **2015**, *20*, 19–29. [CrossRef]
30. Chen, H.; Lv, C. Online Learning-Informed Feedforward-Feedback Controller Synthesis for Path Tracking of Autonomous Vehicles. *IEEE Trans. Intell. Veh.* **2023**, *8*, 2759–2769. [CrossRef]
31. Rajamani, R. *Vehicle Dynamics and Control*; Springer Science & Business Media: Berlin/Heidelberg, Germany, 2011.
32. Sakalli, A.; Aktekin, O.; Kiran, U. Hardware in the Loop (HiL) testing of a human electric hybrid vehicle. In Proceedings of the 2018 IEEE International Conference on Industrial Technology (ICIT), Lyon, France, 20–22 February 2018; pp. 193–198.